Annu. Rev. Astron. Astrophys. 2001. 39:99–136

THE ORION NEBULA AND ITS ASSOCIATED POPULATION

C. R. O'Dell
Department of Physics and Astronomy, Box 1807-B, Vanderbilt University, Nashville, Tennessee 37235; e-mail: cr.odell@vanderbilt.edu

Key Words gaseous nebulae, star formation, stellar evolution, protoplanetary disks

■ **Abstract** The Orion Nebula (M 42) is one of the best studied objects in the sky. The advent of multi-wavelength investigations and quantitative high resolution imaging has produced a rapid improvement in our knowledge of what is widely considered the prototype H II region and young galactic cluster. Perhaps uniquely among this class of object, we have a good three dimensional picture of the nebula, which is a thin blister of ionized gas on the front of a giant molecular cloud, and the extremely dense associated cluster. The same processes that produce the nebula also render visible the circumstellar material surrounding many of the pre–main sequence low mass stars, while other circumstellar clouds are seen in silhouette against the nebula. The process of photoevaporation of ionized gas not only determines the structure of the nebula that we see, but is also destroying the circumstellar clouds, presenting a fundamental conundrum about why these clouds still exist.

1. INTRODUCTION

Although M 42 is not the largest, most luminous, nor highest surface brightness H II region, it is the H II region that we know the most about. The combination of the properties of being the closest H II region, association with a young star cluster that includes massive stars, apparent brightness, and relative simplicity makes it one of the most famous celestial objects and the subject of investigation by almost every new type of observation. This pattern has held true since the advent of the first optical telescopes through today's X-ray observatories. It is no surprise, therefore, that we know more about this one object than probably any other region of recent star formation. The purpose of this review is to establish what we know about the object and its environment, where we will see that our knowledge has increased tremendously in the last few decades. We will also see that there are many remaining questions.

M 42 is a component of the ridge of giant molecular clouds in the constellation Orion, which are part of the Eridanus superbubble of material (Heiles 1998). The long ridge of molecular material extending N–S through the belt of Orion and its sword region is home to several star associations of various young ages, with

M 42 probably being the youngest of these. Even the host cloud (OMC-1) appears to have produced three regions of massive star formation, the most luminous of which has produced M 42, but also nearby are imbedded groupings to the NW and SW of the tight clustering of early type stars known as the Trapezium. The historical interest in this region continues through the present, with over one hundred papers on Orion being published annually in refereed journals.

There have been major reviews of our knowledge of the object, two outstanding examples being the compilation of material by Goudis (1982) into a source book and the proceedings of the symposium marking the centennial of the first photographic images of M 42 (Glassgold et al. 1982). Earlier volumes of this publication have presented review articles covering various closely related subjects, which include the evolution of H II regions (Mathews & O'Dell 1969, Yorke 1986), the molecular cloud and its associated stars (Genzel & Stutzki 1989), the process of star formation in molecular clouds (Evans 1999), the structure and evolution of the underlying photon dominated region (Hollenbach 1997), and the revealing new X-ray observations (Feigelson 1999). The Astronomical Society of the Pacific has published two short reviews on the nebula and its physics (Ferland 2001, O'Dell 2001a). For reasons of brevity, the reader is referred to these articles for subjects not immediately related to the nebula and its associated population.

Although M 42 can be argued to extend to almost one half degree in angle, most of the radiation comes from the inner few arcminutes, a region referred to as the Huygens region after the observer who first recorded its appearance (Gingerich 1982). This is a complex region and the reader is advised to study the map provided in Figure 1 and the detailed optical high resolution image shown in Figure 2.

2. THE STRUCTURE OF M 42

2.1 Evolution to the Current Model

The basic model for M 42 is that of a thin concave blister of photoionized material on the portion of the surface of OMC-1 facing the Sun, with the emitting layer being thin ($\simeq 0.1$ pc) as compared with the lateral dimension ($\simeq 1$ pc). This simple picture is quite different from earlier views, when the modeling process was strongly affected by Strömgren's (1939) influential general argument for ionized spheres. Although the approximately circularly symmetric surface brightness distribution does not match that of a constant density gaseous sphere, it does suggest radial symmetry in three dimensions. The most sophisticated version of such a model is that of Osterbrock & Flather (1959). They employed the diagnostic tool of observing the [O II] 3727 Å doublet ratio to determine the line-of-sight spatial electron density n_e, together with the extinction-free surface brightness in radio wavelength free-free emission. These determined a model where the nebula was spherically symmetric and had a radially decreasing n_e, but they had to introduce a volume filling factor to reconcile the two sets of observations. Such a radial model was used to derive the gas to dust ratio (O'Dell & Hubbard 1965) that is

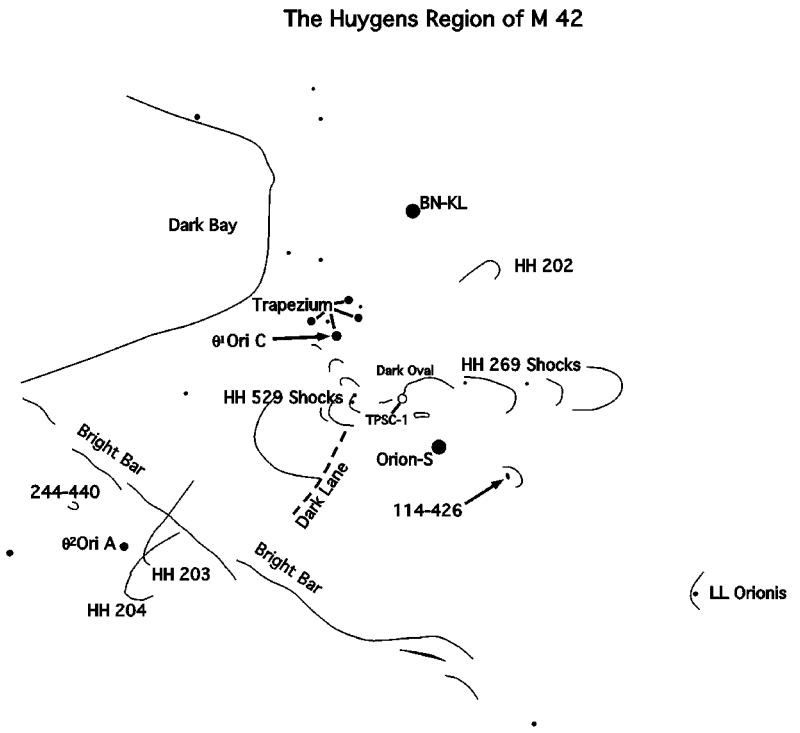

Figure 1 This drawing mimics the field of view of many of the succeeding images. It presents the commonly accepted names for many of the features discussed in the article.

still widely used, although the results are no better than the now discredited model used in their derivation. However, even while the spherically symmetric model was being widely assumed, alternative views were being presented. Münch (1958) interpreted observations of the small scale variations of radial velocity as an argument that the optical nebula is a relatively thin slab, explaining this structure as a result of the emitting material being optically thick due to the imbedded dust. A similar conclusion was reached by Wurm (1961) from his quantitative photographic images. The Wurm model was strongly disputed by Münch & Wilson (1962). From a comparison of the surface brightness of the nebula in the He I 3889 Å line with the column density of He I calculated from the equivalent width of that line in the Trapezium stars, they argued that the nebula was composed of many extremely small condensations. During the period of this debate there was a continuously improved set of observations of the radial velocities of the optical emission lines and theoretical hydrodynamic models (Mathews 1965, Lasker 1966, Mathews & O'Dell 1969). Kaler (1967) showed that there was a systematic trend in the radial velocities, with the higher states of ionization (which must arise from regions closer to the dominant photoionizing star θ^1 Ori C) being more

blueshifted. θ^1 Ori C is the brightest of the four Trapezium stars. The velocity trend was inconsistent with a spherically symmetric nebula and was used independently and essentially simultaneously by Balick et al. (1974) and Zuckerman (1973) to come up with today's model. In a simple manner, the assumption of a thin emitting layer of radially decreasing density lying beyond the ionizing star reconciles the three primary characteristics of surface brightness, n_e, and radial velocity shifts.

Understanding the radial velocity variations requires a basic understanding of photoionization (PI) theory and the associated hydrodynamics. First order PI theory recognizes (Osterbrock 1989, O'Dell 1998b) that the ultraviolet opacity is dominated by the two most abundant elements, hydrogen and helium. This has the consequence that the distribution of the ionic states of the heavy elements that produce much of a nebula's radiation through collisional excitation of forbidden lines, is determined by the hydrogen and helium opacities. This means that regions closest to θ^1 Ori C will have a He^+ zone that will also host the O^{++}, which gives rise to [O III] 5007 Å. Further away, there will be a He^o zone that will also contain O^+ that gives [O II] 3727 Å emission and N^+ that gives the [N II] 6583 + 6548 Å doublet. The furthest layer is the ionization front proper, where hydrogen transitions from its fully ionized condition in the He^+ and He^o zones to neutral. The ionization front is well delineated by both the [O I] 6300 + 6363 Å and the [S II] 6717 + 6731 Å doublets, because only that thin region (about 10^{-5} pc thick) combines the presence of thermalized electrons coming from the photoionization of hydrogen with these low ionization potential ions. The more refined CLOUDY code program (Ferland et al. 1998) shows that this hydrogen plus helium opacity driven model is indeed only a first order approximation. However, it does give the basic ionization structure (Baldwin et al. 2000). In the case of photoionization by θ^1 Ori C, the absence of detectable He II recombination lines indicates the absence of a significant doubly ionized helium zone (Baldwin et al. 2000). In a slab model, PI will produce an overpressure situation due to both ionization and heating. Material will flow at about the sonic velocity ($\simeq 17$ km s^{-1}) away from the ionization front and towards θ^1 Ori C, with emissions from the different ionization zones that will have various velocities. A compilation of the relevant velocities (O'Dell 1994), showing the expected velocity-ionization zone behavior is given in Table 1.

TABLE 1 The ionization front behind θ^1 Ori C

	Key ion	**Markers**	$V_\odot$ **(km s^{-1})**	**Density (cm^{-3})**	**Depth (pc)**
PDR	H^0	CO, C II	28	10^5	?
IF	H^+	[O I], [S II]	25.5	$\geq$6000	10^{-4}
Low ionization	He^0	[O II], [N II]	18.8 ± 1.5	7000	2×10^{-3}
Medium ionization	He^+	[O III], H II, He I, [Cl III]	17.9 ± 1.3	4000	0.06

Velocities are from Goudis (1982), O'Dell & Wen (1992), Hu (1996a). Densities are from Tielens & Hollenbach (1985), Escalante et al. (1991), Pogge et al. (1992), Jones (1992), and Walter (1993). IF and low ionization depths are from O'Dell (1994) and Wen & O'Dell (1995).

Heliocentric velocities will be used throughout this review, these values being 18.1 km s^{-1} more positive than M 42 velocities in the Local Standard of Rest.

A complete PI model of a freely expanding blister nebula would incorporate both the effects of the heating and cooling processes arising from PI, and also the dynamical effects of the gas accelerating, and the density dropping away from the ionization front. Such a model does not now exist. However, a static blister model was calculated by Rubin et al. (1991) under the assumption that the ambient gas density dropped exponentially in the direction perpendicular to the plane, the ionization zone being formed within this ad hoc density structure. This model matches the main ionization characteristics of the nebula in that it has no He^{++} zone because of the low temperature of θ^1 Ori C. Also, the He^o zone is quite narrow, but it did not provide a good match to observed line ratios outside of the central region. A more self consistent model was calculated by Baldwin et al. (1991) using the CLOUDY (Ferland et al. 1998) PI program, with which one calculates the expected equilibrium density. The program includes many more terms in the calculation, especially the important role of imbedded interstellar dust. This model produces better agreement with observations. That these two models agree with observations as well as they do reflects the fact that the density distribution expected from a freely expanding slab ionized from one side will approximate an exponential drop (Hester et al. 1996). However, the CLOUDY model produces a static model for the nebula. The restricting force is produced by stellar radiation pressure pushing on the imbedded grains. Because it is well established that there is expansion away from the main ionization front, this means that one of the basic assumptions of the CLOUDY calculations has not been satisfied, or that the grains are slipping through the ambient gas (Ferland 2001). The ultimate theoretical model will include not only all the physics of PI and the hydrodynamics, but also the curvature of the ionization front discussed in the next section.

2.2. The 3-D Structure of the Main Ionization Front

Since the main ionization front (MIF) is a wall that is eating its way into OMC-1 through the process of photoevaporation, one would expect it to have progressed furthest from θ^1 Ori C at the substellar point, and to have been retarded in portions of high ambient density within the molecular cloud, i.e., one would not expect the nebula to be a simple slab. Fortunately, there is a way of approximately calculating the current structure.

Ferland pointed out in the Baldwin et al. (1991) paper that there should be a linear relation between the surface brightness in a recombination line of H I and the flux of photoionizing photons from the ionizing star. This statement reflects the fact that along any one line of sight from θ^1 Ori C ultimately all Lyman continuum photons will be absorbed, producing an ionization of a hydrogen atom. This will eventually recombine, giving rise to easily observed emission lines such as Hα and Hβ. This consequence is rigorously true only if no new atoms are being photoionized at an important rate. This is the case in M 42. The observed surface brightness will linearly scale with the ionizing flux only when the line of

sight passes through the ionizing star. This is true only at the substellar point for a distant observer. Nevertheless, using simple assumptions about the geometry, Baldwin et al. (1991) could explain the general drop of surface brightness with increasing angular distance from θ^1 Ori C.

This mechanism was applied more rigorously by Wen & O'Dell (1995), who adopted the spatial density distribution determined by Pogge et al. (1992) and rigorously calculated the distance of the MIF front from θ^1 Ori C point by point across the nebula. They assumed a local exponential density distribution away from the MIF and pointed out that for such a distribution there will be important simple relationships with the thickness of the emitting layer (l) calculated from the extinction corrected surface brightness under the assumption of a constant density. In this case, the scale height, a, for the density drop will be $l/2$. Because the emissivity varies as the square of the density, the emissivity will drop exponentially with a scale factor $l/4$. The derived l is about 0.1 pc for the central region of M 42 (Pogge et al. 1992, Wen & O'Dell 1995). This corresponds to 46″ at M 42's distance of about 450 pc (Warren & Hesser 1977, Genzel et al. 1981, Brown et al. 1994). This means that the emissivity is dropping with a scale height of about 12″. For reference, θ^1 Ori C lies 135″ northwest of θ^2 Ori A, the comparably bright 09.5 Vp star lying to its SE. The beauty of the application of Ferland's mechanism is that, given enough information, one can calculate the 3-D structure of the MIF, although the method of calculation progresses radially, so that errors in the inner part will propagate outwards. The resultant model is shown in Figure 3, where data behind the Dark Bay feature have been approximately interpolated using the results from radio observations of Wilson et al. (1997). The distance between θ^1 Ori C and the substellar MIF is about 0.25 pc, and the surface curves

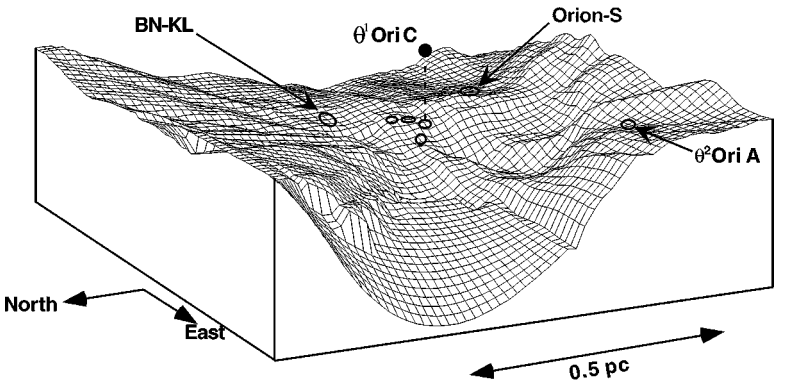

Figure 3 A three-dimensional depiction of the surface described by the MIF derived by Wen & O'Dell (1995), as amended with radio emission line observations (Wilson et al. 1997) is shown. The relative position of θ^1 Ori C is shown by a filled circle, and the projection onto the MIF of major stars and infrared sources is shown by open ellipses. The Sun's position is at 450 pc on the vertical axis.

upward to the plane of the sky containing the star at a characteristic distance of 0.5 pc.

2.3. The Foreground Veil

The Dark Bay is the best illustration that there are regions of visual wavelength high optical depth between the observer and the MIF. The fact that it is extinction and not an absence of emission is established by the continued recombination radio emission in that area (Wilson et al. 1997). Those radio observations have been used to fill in the Dark Bay region of the 3-D model of the MIF in Figure 3. Most recently, the foreground extinction has been derived at about 1.5″ resolution across the brightest parts of the nebula by comparing the Hα surface brightness with 20-cm radio emission (O'Dell & Yusef-Zadeh 2000). Figure 4 is a map of the derived extinction, expressed in terms of $c_{H\beta}$ as the base ten logarithm of the transmission at 4861 Å. One sees here that the entire nebula suffers from extinction. There are numerous knots within the Dark Bay region. The largest of these have a mass of about 0.01 $M_\odot$ if the gas to dust ratio is like the general interstellar medium. The western tip of the Dark Bay is marked by a sharp bow shock that forms a dark wisp.

That this extinction is associated with the near–M 42 region, rather than being foreground, is established in two steps. An extremely important paper of van der Werf & Goss (1989) determined the column density of neutral hydrogen at a

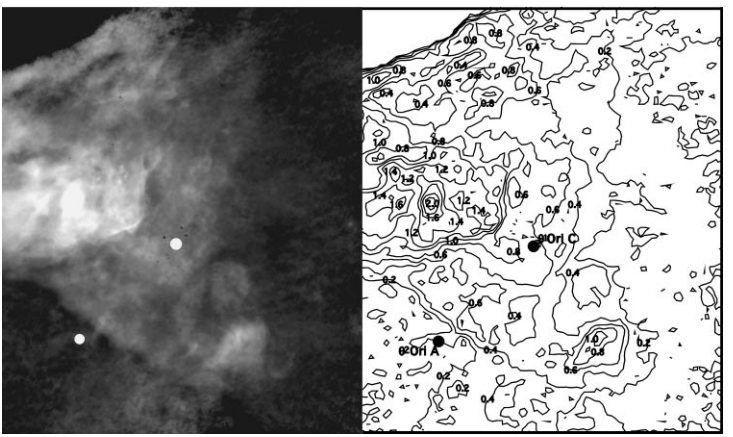

Figure 4 The left figure shows an image of the extinction coefficient $c_{H\beta}$ over a range of values from 0–1.6. The right hand image is a contour plot of the same area in steps of 0.2 in units of dex(10). Both images are the full field of Figure 1. The contours were determined with a resolution of 3″. The occasional small dark spots are scars of bright stars where the original image was saturated (O'Dell & Yusef-Zadeh 2000). The lack of data at the top left corners indicates where the observed surface brightnesses were too low to derive extinctions.

resolution of 18″ by measurement of the 21-cm line in absorption against the nebular continuum originating from close to the MIF. The absorption line was saturated within the Dark Bay feature, but in the other regions, column densities could be determined out to where the radio continuum became too weak. A subsequent comparison of extinction derived from the Balmer decrement with the neutral hydrogen column densities (O'Dell et al. 1992) established that the extinction and HI column density were closely correlated, meaning that the same material was causing the extinction and the 21-cm absorption, and that the dust to gas ratio values were about the average for the general interstellar medium. van der Werf & Miller found that the hydrogen was grouped into three preferred velocities; system A (24 km s^{-1}, range of 22–25 km s^{-1}), system B (21 km s^{-1}, range 18–22 km s^{-1}), and system C (16 km s^{-1}, range 13–19 km s^{-1}). Although the velocity ranges almost overlap, they argue from the most frequent values and the different distributions that there are indeed three systems, progressively blueshifted from the OMC-1 velocity of 28 km s^{-1}. Arguments in support of the reality these three velocity systems come from measurement of Na I and Ca II absorption lines in the spectra of the Trapezium stars and in θ^2 Ori A (O'Dell et al. 1993a). The optical studies show that there are additional but weaker velocity systems, the strongest of which is at 8 and 1 km s^{-1}. van der Werf & Goss (1990) also found multiple unresolved and partially resolved discrete 21-cm absorption blueshifted features at velocities of 1 to 8 km s^{-1} and one quite faint feature at 27 km s^{-1}. They interpret the blueshifted (with respect to OMC-1) features as cloudlets accelerated by the rocket effect; however, this is probably not the case because it would mean that the photoionization that produces the rocket effect would also produce optically bright surfaces on the cloudlets. None are seen. We shall see later that there is ample evidence for jet driven shocked material in the foreground material, selectively causing small blueshifted components. These may be the driving source for these cloudlets.

The various systems taken together are frequently called the M 42 lid, but the term "veil" is probably more accurate, since it is at least partially transparent. The similarity of the velocities to OMC-1 and the expected absence of similar velocities in that direction within the Milky Way Galaxy argues for a direct association with OMC-1 and possibly with M 42. However, one cannot accurately place this veil material with respect to θ^1 Ori C and the nebula. Because it is neutral material, there should be an ionization front on the side facing θ^1 Ori C. This has not been detected. This could be due to the lid being far removed from high Lyman continuum fluxes, or to material flowing away (redshifted in this case) from the neutral material, and the corresponding optical lines are lost in the much stronger blue shifted emission from material near the MIF. If one adopts the three-dimensional distribution for the Orion Nebula Cluster (ONC) stars of Hillenbrand & Hartmann (1998), and the fraction of stars that are silhouette type proplyds (Section 6.1) of Bally, et al. (2000), then the veil is at a distance of about 0.6 pc from θ^1 Ori C. A depiction of the M 42 region is shown in Figure 5. This image was rendered by the San Diego Supercomputer Center under contract with the American Museum of Natural History as part of the Three-D Galaxy project of

the new Hayden Planetarium. It is based on the Wen & O'Dell (1995) 3-D model, the extinction corrected HST mosaic image (Figure 6), and the placement of the veil, stellar, and shock components as per this article.

2.4. Structure in the MIF

The predominant intrinsic structure in the MIF is the Bright Bar (see Figure 1). This was originally proposed by Balick et al. (1974) to be an escarpment in the MIF on the basis of the enhancement of the low ionization features like [S II] and [N II] emission. We are probably viewing the MIF almost edge-on along the Bright Bar. This interpretation has been verified by a series of infrared and radio observations which measure material that lies beyond the MIF. The object and its neutral zone physics is well described by Tielens et al. (1993). They point out that the progression of peak emission agrees well with their model for a Photodissociation Region (PDR, Hollenbach & Tielens 1997). Using the acronym PDR is especially convenient since various authors refer to the PDR as being the Photon Dominated Region and the Photodissociation Region. Immediately behind the MIF one finds a peak of emission of hot particles, heated by θ^1 Ori C's photons of less than 13.6 eV. Further out is a zone of peak H_2 emission and beyond that is the CO peak. More recent observations have detailed this region in additional atoms and ions (CI, Tauber et al. 1995; CO, Tauber et al. 1994; $H_2CO + CS$, Hogerheijde et al. 1995; $HCO^+ +$ HCN, Young Owl et al. 2000) while these results indicate that the PDR behind the Bright Bar must be highly clumped (Jansen et al. 1995). PDR emission should be occurring throughout M 42 from behind the MIF, but it is only at the Bright Bar that one has the edge-on view that allows separation of its various layers. The surface brightness of the nebula drops precipitously outside of the Bright Bar. This is understandable within the framework of the Ferland mechanism because that region is much flatter than the MIF closer to θ^1 Ori C. There is evidence that the Bright Bar is not quite this simple. Walmsley et al. (2000) draw on their recent infrared spectroscopy to argue that the underlying structure is cylindrical, rather than flat. Moreover, one sees quite narrow features, which are thought to be limb-brightened portions of the MIF, but some of these seem to show the ionization gradient in the wrong direction, if θ^1 Ori C is the source of ionizating photons for all of this region. It is entirely possible that θ^2 Ori A's radiation is complicating the picture; however, the primary characteristic that the Bright Bar is caused by a straight escarpment in the MIF is probably correct. Like the other large scale features in the MIF, this must be due to a corresponding density enhancement in OMC-1.

An extinction corrected image (Figure 6) of M 42 (O'Dell & Yusef-Zadeh 2000) reveals that there are numerous additional linear bright features. A determination of the variation of the surface brightness ratios in high and low ionization lines indicates that they have the same structure as the Bright Bar, i.e., these are features caused by local escarpments. Large-scale linear features are difficult to form in the underlying OMC-1 neutral zone, so the origin of these features remains unknown. Typically such an escarpment will produce lower surface

brightness regions outside of them, which explains many of the dark nearly linear structures in the extinction corrected image, but there is one such feature (labeled Dark Lane in Figure 1) that does not have the associated ionization ratio changes associating it with an escarpment. Figure 6 also shows nicely a 60″ filled circle of enhanced [O III] emission to the WSW from θ^1 Ori C. Hu (1996a) has shown that this is associated with O^{++} redshifted by 22 km s^{-1} with respect to OMC-1. Its nature is unknown, although the fact that it lies close to the axes of the blueshifted Herbig Haro objects HH 202, 203, and 204 suggests excitation by shocks. The extinction-corrected image also shows that the sharply defined dark arc to the SW from θ^1 Ori C is not a simple extinction feature, a property shared by the rectangular dark feature immediately south of it. O'Dell & Yusef-Zadeh (2000) intepret the dark arc as a well defined escarpment caused by outflow from an imbedded source in the Orion-S region.

An additional feature associated with material in or near the MIF is the low temperature Ney-Allen (1969) infrared source lying a few seconds of arc to the SW from θ^1 Ori D (Hayward et al. 1994). This is a broad arc of emission that is probably produced by particles heated by θ^1 Ori D due to that star lying much closer to the MIF than the other bright members of the Trapezium, an argument strengthened by the fact that θ^1 Ori D has an absorption line component identifiable with the MIF and absent in the other members (O'Dell et al. 1993). Unlike the BN-KL and Orion-S strong infrared sources shown in Figure 1, this is not thought to be a center of recent star formation and associated molecular outflow.

A final feature that is not seen directly, but was posited by Pankonin et al. (1979), is a central stellar-bubble cavity caused by the stellar wind of θ^1 Ori C. The wind has been determined by Howarth & Prinja (1989) to be losing 4×10^{-7} $M_\odot$ yr^{-1} at 1000 km s^{-1} from UV spectroscopy of the star. The Pankonin et al. arguments are based on local variations in the radial velocity of the H 76α emission, but the angular resolution was only 1′. There is no direct evidence of such a windblown cavity. The enhanced [O III] disk of Hu is not associated, as its center is well displaced from θ^1 Ori C. One does see indirect evidence of the wind in the stand-off shocks formed near the proplyds closest to θ^1 Ori C, as discussed in Section 7.3. There may be evidence for a wind-blown cavity in the observations of the HeI 3889 Å absorption line in the stellar spectra. This line is formed (Münch & Wilson 1962) in the metastable 2^3S state of He^o, which is populated by recombinations of He^+. Since the nebula is bright in both that emission and the other strong optical line arising from the same level (10830 Å), one can get contamination-free absorption lines in only a few of the stars (θ^1 Ori A, θ^1 Ori C, θ^1 Ori D, θ^2 Ori A) (O'Dell et al. 1993). All of these stars have strong 3889 Å absorption components near 2 km s^{-1}. θ^1 Ori D shows an additional less strong feature at 20 km s^{-1} and θ^1 Ori D shows a similar strength feature at -30 km s^{-1}. Because the 2 km s^{-1} feature is seen in the more distant θ^2 Ori A, it is unlikely to be associated with a stellar-bubble. Moreover, that component has matching Na I and Ca II absorption features. It is argued by O'Dell et al. that this velocity system lies on the observer's side of the foreground neutral veil of material. These authors argue that the two additional

components seen in θ^1 Ori D and θ^1 Ori C are material accelerated by θ^1 Ori C's stellar wind.

3. ANALYSIS OF THE NEBULA'S RADIATION

3.1 Derived Abundances and the t^2 Problem

The broadest application of the results of studying M 42's emission lines is arguably the comparison of its relative abundances to those of other H II regions in our and other galaxies. Since the physical processes occurring here must also apply there, what we determine from the detailed study of M 42 must also apply elsewhere. The slowness in converging to accepted abundances in M 42 is a cautionary note to students of other H II regions, which cannot have their physical properties determined as accurately. At this point there is a quite complete set of the optical lines reaching as faint as 10^{-4} of the intensity of Hβ (Baldwin et al. 1991, Osterbrock et al. 1992, Esteban et al. 1998, Baldwin et al. 2000), and ultraviolet (Bohlin et al. 1980, Walter et al. 1992, Rubin et al. 1998), and infrared (Simpson et al. 1986) lines to brighter limits.

The emission lines we observe are primarily produced by two processes, recombinations following photoionizations, and spontaneous decay through forbidden line emission following collisional excitation. These two processes are well understood and are described clearly in the literature (Osterbrock 1989). [O I] lines, such as that at 8446 Å can be produced by resonance fluoresence pumping of upper levels of O^0 by the abundant hydrogen Lyβ photons (Swings 1955, Münch & Taylor 1974). More importantly, [Fe II] lines can result from absorption of stellar continuum photons, a process also invoked to explain the recently discovered deuterium lines (Hébrard et al. 2000a,b). The key parameter in determining the emissivity of emission lines through the primary two processes is the electron temperature (T_e). The optical recombination lines increase in their emissivity with decreasing T_e, whereas collisionally excited lines increase in emissivity almost exponentially with increasing T_e. This means that if the line of sight into the nebula is not homogeneous, then recombination and collisionally excited lines will selectively come from different regions, thus complicating the abundance analysis.

3.1.1. THE t^2 PROBLEM The fact that sampled lines of sight into M 42 are not homogenous in temperatures was first established by Peimbert (1967). As a measure of this inhomogeneity he introduced the square of the electron temperature dispersion about its mean value $t^2 = (\Delta T_e/T_e)^2$. For M 42 $t^2 \simeq 0.03$ (Esteban et al. 1998), which means that the temperature fluctuates by about 1600 K about the equilibrium value of 9200 K. Recombination processes, such as the Balmer continuum, produce temperatures as low as $T_e \simeq 6900 \pm 700$ K (Liu et al. 1995), while collisional lines give higher temperatures ($T_e \simeq 9200$ K, Baldwin et al. 1991). In Esteban et al's position 1, they found a strong progression of T_e from different ions, deriving T_e([S II]) $= 10300^{+2440}_{-960}$ K, T_e([N II]) $= 9850 \pm 375$ K,

and T_e([O III]) = 8300 $\pm$ 210 K, and, from the Balmer lines-to-continuum ratios $T_e = 8730 \pm 800$ K, i.e., a notable increase in T_e as one approaches the main ionization front. Wilson et al. (1997) determine $T_e = 8300 \pm 200$ K from the ratio of the 64α line to its adjacent radio continuum. This progression generally agrees with that expected from the hardening of the radiation field because the lowest energy photoionizing radiation is removed first.

The origin of these temperature fluctuations is not yet established. To an accurate first approximation, the heating rate is dependent upon the product of the square of the density and the average excess energy of the absorbed photons, whereas the cooling processes are dependent on the square of the density. This means that the density drops out of consideration, especially at the densities associated with the MIF, so that inhomogeneities of density cannot produce the fluctuations in T_e. A secondary source of heating is the photoelectric ejection of electrons from grains, which will depend only on the first power of the density of these particles. This means that if there are grain rich or grain poor regions in the nebula, this can contribute to t^2 (Mathis 1995, Ferland 2001). The large scale variations in T_e seen by Liu et al. (1995), the presence of regions heated by shocks (Peimbert et al. 1991), and regions shielded from direct illumination by θ^1 Ori C (O'Dell 2000) can also contribute.

3.1.2. ABUNDANCE OF ELEMENTS IN ORION Relative abundances of the gas in M 42 are derived from emission line ratios. Given the existence of the t^2 problem, the most accurate abundances come from lines that are produced by the same emission mechanism, recombination or collisional excitation. The preferred method is a comparison of recombination, lines because of the lower dependence upon electron temperature. Because the heavy ion recombination lines are usually quite weak compared with H and He lines, their accurate measurement demands high spectral resolution. This same high resolution is also important in the study of the auroral transitions of [O I] and [N II] because the nebular lines can be much weaker than foreground night sky emission. This requires observations at high velocity resolution when the relative velocity of the observer and nebula are greatest. Most of our knowledge of abundances derives from optical window CCD spectra, there being three recent independent and complementary investigations. Osterbrock et al. (1992) covered the full optical window (3180–11000 Å) at a resolution of about 360 km s^{-1} and found 222 lines. Esteban et al. (1998) covered 3500–7060 Å at 30 km s^{-1} and measured 220 lines, while most recently Baldwin et al. (2000) covered 3498–7468 Å at 10 km s^{-1} and measured 444 lines of intensities down to 10^{-4}, that of Hβ. Ultraviolet (e.g., Rubin et al. 1998), and infrared (e.g., Lester et al. 1977, Simpson et al. 1986) spectra have also been useful, even though the subject is driven by the rich available optical spectrum. A notable exception is the accurate derivation of N/O from infrared lines (Rubin et al. 1988) where the method is quite insensitive to T_e. One works from the observed lines and then draws upon the theoretical models to correct for those few cases where ionic states with significant fractions of the total population are not observed. In some cases the observed lines are produced by fluoresence pumped by the stellar continuum

(Grandi 1975a,b), where the derivations become more complex. The best example of continuum fluorescence is the [Fe II] spectrum, where many of the lines of the rich spectrum are primarily produced by this mechanism (Verner et al. 2000). Recognition of the importance of this process and the availability of auroral transition [O I] line, fluxes accurately corrected for night sky emission (Baldwin et al. 1996, 2000, Verner et al. 2000) has resolved the anomalies in the [Fe II] spectrum. Resolution of the anomalies has eliminated the need for including many high density ($n_e = 10^6$ cm^{-3}) knots within the primary emitting layer (Bautista et al. 1994).

The most complete analysis is that of Esteban et al. (1998), who used a wide variety of collisionally excited and recombination lines. The results for the logarithm of the relative abundances (normalized to log $N_H = 12.0$) are for He(10.99 $\pm$ 0.02), C(8.39 $\pm$ 0.06), N(7.78 $\pm$ 0.08), 0(8.64 $\pm$ 0.06), Ne(7.80 $\pm$ 0.10), S(7.17 $\pm$ 0.10), Cl(5.33 $\pm$ 0.15), and Ar(6.80 $\pm$ 0.20). Esteban et al.'s iron abundance (6.41 $\pm$ 0.20) derived from Fe^+ and Fe^{++} observations together with a correction factor for Fe^{+3} agrees well with derivation of Verner et al. (2000). Their key diagnostic abundance ratio of N/O (0.14) agrees well with the $N^+/O^+ = 0.14$ value derived from ultraviolet observations (Rubin et al. 1998). This is not unexpected because the singly ionized emission arises primarily from the He^o zone.

These abundances are for the gaseous phase of material in the main ionization zone of M 42. There is evidence that the major fraction of some heavy elements, e.g., Ca, Al, Fe, Mg, Si, is trapped in the dust grains. Esteban et al. (1998) argue that this depletion is about eight times when compared with the true abundance in the Orion region (taking the dust free atmospheres of the stars as the point of reference). Since these elements trapped in grains will also trap a certain fraction of elements like carbon and oxygen, corrections must be applied to the gaseous abundances in order to get the total abundance of each element (Savage & Sembach 1996). This gives results comparable to the abundance of C, N, and O in the stars of the Orion association stars (Cunha & Lambert 1994) and with the fact that the metallicity of Orion is about two-thirds that of the Sun (Baldwin et al. 1991, Esteban et al. 1998). This presents a challenge for interpretation through simple models for Galactic chemical enrichment, since Orion represents today's sample of the gas from which stars are being formed. This should be richer in heavier elements than the 4.5 Gyr old Sun (Pagel 1997). However, the complexity of enrichment of the gas and subsequent new stars is illustrated by the fact that pre–main sequence F-G and main sequence B stars have similar Fe abundances, but there is a star-to-star variation in the F-G oxygen abundance (Cunha et al. 1998). The fact that the depletions of Fe, Mg, and Si are not as great as in the general interstellar medium is an argument that dust grains are being destroyed in the ionized zone, rather than being removed by forces such as radiation pressure.

3.2. Deuterium in M 42

In the general Orion region the D/H abundance ratio is about 0.9×10^{-5} (Jenkins et al. 1999, Laurent et al. 1979, Bertoldi et al. 1999, Wright et al. 1999). This is marginally lower than the solar neighborhood value of 1.6×10^{-5} (Piskunov et al.

1997). The first identification of D emission lines in the optical spectra of M 42 was made by Hébrard et al. (2000a), measuring the isotopically shifted (-82 km s^{-1} when both H and D come from the same velocity system) Dα and Dβ lines. The successful identification pivots about recognition that the D and H lines are not coming from the same velocity system, the D lines being produced in the PDR region at -28 km s^{-1}. Dα was in fact previously observed in a search for D (Traub et al. 1974), but it was confused with Hα emission from the numerous high velocity components known to mark M 42. It was also seen in the blue shoulder of the Brγ line (Oudmaijer et al. 1997), but not recognized because they could see no corresponding component in Hβ at their signal-to-noise ratio. The reality of the identification is confirmed in two ways, first, that there are no similar components in [N II], [O II], or [O III] lines (Hébrard et al. 2000b) and secondly, that the D line ratios (within the equivalent of the Balmer series) are quite different from what is expected for PI and recombination. Hébrard et al. (2000a) correctly argue that the most likely mechanism of excitation of the levels producing the D emission lines is fluoresence by the continuum of θ^1 Ori C in the blue profiles of the stellar Lyman lines. This radiation will primarily come from regions of the PDR that are close enough to the MIF to remain optically thin to the UV stellar continuum. In effect, the near MIF portion of the dense PDR is acting as an absorbing layer for producing D lines through cascades following photoexcitations. More extensive observations of deuterium in the Orion Nebula have been reported by O'Dell et al. (2001), who report similar, but not identical, results. They present a detailed model for explaining the strength of the D emission lines and how the D/H line intensity ratio should vary in different members of the Balmer series. They also establish that fluorescence excited D emission lines do not offer the possibility for determining the D/H abundance ratio.

3.3. The Role of Scattered Light

The continuum radiation in M 42 is much stronger than that expected from purely atomic processes. The magnitude of the discrepancy began to be quantified with photographic images. It was then precisely determined by photoelectric filter photometry (O'Dell & Hubbard 1965) and with essentially identical results by low resolution CCD spectrophotometry (Baldwin et al. 1991). In the central region the observed equivalent width (the interval of the underlying continuum necessary to produce the same amount of energy as in the emission line) of Hβ is about 500 Å, whereas the expected atomic continuum would be 1900 Å. The equivalent width decreases outward, becoming about five times less in the outermost regions, so that at large distances the emission from the nebula is dominated by the extra continuum (O'Dell & Hubbard 1965), which is scattered starlight. Even in the inner regions the continuum of the nebula has to be considered to be a combination of reflection and emission line processes; however, the former characteristic doesn't affect the analysis of the emission lines since it is simply subtracted as background. An important limitation to that statement is discussed later in this subsection. At this point, the scattered light continuum has been characterized from the visual

through the near ultraviolet (Peimbert 1967, Hua 1972, Perinotto & Patriarchi 1980, Mathis et al. 1981, Onaka et al. 1984, Patriarchi & Perinotto 1985). Further confirmation of the importance and origin of the excess continuum is shown in polarimetric studies of the nebula. The optical continuum linear polarization has been shown to be at the level of a few percent (Isobe 1977, Pallister et al. 1977). The electric vectors are perpendicular to the radius vector from the Trapezium, establishing it as scattered light from those stars. This property can then be used to estimate the distance between the Trapezium stars and the primary scattering layer (O'Dell 1994), which we will see is the Photon Dominated Region (PDR). The true polarization of the scattered light portion of the continuum becomes as high as 20% 30″ west of θ^1 Ori C (Leroy & Le Borgne 1987), which is much higher than that predicted for the scattering particles occurring both around the star and in a background slab (White et al. 1980) and they find that Hα and [O III] 5007 Å emission is also polarized, although much less than the scattered light continuum.

3.3.1. WHERE THE LIGHT IS SCATTERED AND THE NEBULA'S OPTICAL DEPTH The important questions are where is the dust that is producing the scattered light and is it sufficiently plentiful to make the nebula optically thick? If the answer to the latter is yes, then the dust will determine the optical appearance of the nebula, a position advocated by Münch in multiple papers. This assumption also underlies the modeling by Mathis and his students. Unfortunately, scattered light observations are not powerful model discriminants (White et al. 1980), and models that assume optical thickness can produce some of the observed properties of the nebula. Münch has eloquently advocated the optically thick model (Gómez Garrido & Münch 1984, Münch 1985). The strongest argument for self-extinction comes from observations of the logarithm of the flux ratios of Hα/Hβ and Hβ/Hγ (Münch & Persson 1971). In the case of foreground extinction, the slope of various observed points (each having a different amount of extinction) would be close to 0.30, whereas their observed slopes for different directions averaged 0.225. This is the sense of deviation expected for self-extinction (Leibowitz 1973). However, the Münch & Persson flux ratios seem to be incorrect, since they do not progress back to the well defined theoretical line ratios at low extinctions, a characteristic that can be understood from the method of obtaining the observations. Modern observations of these line ratios indicate good agreement with recombination theory at low optical depths and fall along a slope in the line ratio diagram that is in agreement with foreground extinction (O'Dell 2001b). Further arguments for the extinction primarily being foreground is the fact that the derived extinction for the Trapezium stars ($A_V = 1.55$ mag, Johnson 1967) is in close agreement with the extinction ($A_{H\beta} = 1.5$ mag) derived from the surface brightness in the radio continuum and Hα (O'Dell & Yusef-Zadeh 2000). A major limitation of the self-extinction model is that it does not explain the velocity gradients and ionization structure inferred from line ratios. The original quantitative arguments seem to be flawed and the model fails to explain the modern observations of velocity and line ratios. Hence, it is appropriate to not consider the self-extinction model further.

3.3.2. DEVIATIONS FROM THE "NORMAL" PROPERTIES OF DUST There is significant impact of adopting a blister type, low self-extinction model. In such a model the scattered light will largely occur in the high density PDR immediately beyond the MIF, and the extinction will occur primarily in the foreground veil. The reality of this model means that the scattered light models that assumed significant self-extinction or scattering of light from near θ^1 Ori C cannot be accepted as guides in interpreting the scattered light. Therefore, one is forced to recalculate scattering predictions that take into consideration the curved shape of the PDR, which is probably shaped like the MIF.

It is well known that the Orion Nebula Cluster (ONC) has a deviant extinction curve (Baade & Minkowski 1937, Costero & Peimbert 1970, Cardelli & Clayton 1988, Greve et al. 1994). The blister model means that one cannot invoke local properties of material within the H II region (Sorrell 1992, Cardelli & Clayton 1988) or modifications of the grains due to being close to the stellar wind or intense radiation field of θ^1 Ori C. Since most of the extinction occurs in or near the foreground veil, this means one must look to deviations in the size of the particles there. In the blister nebula model for M 42 one cannot derive a dust to gas ratio. Most of the scattered light is coming from the high density background PDR, and this is what vitiates O'Dell & Hubbard's 1965 values. However, in their study of the extinction, O'Dell & Yusef-Zadeh (2000) show that if the dust to gas ratio were that of the general interstellar medium, the amount of internal extinction along a column looking directly at the MIF would be $A_V \simeq 0.65$ mag. Since essentially all of the extinction in the Trapezium stars can be accounted as due to foreground material (because of its near equality with the nebular extinction in spite of the fact that θ^1 Ori C must lie well in the foreground of the blister), one can conclude that dust to gas ratio in the nebular material is less than the global average. It is well established that aluminum, calcium, and magnesium are well depleted compared with stellar abundances (Kingdon et al. 1995). This phenomenon is also present in the general interstellar medium, and is likely to be due to these elements being selectively tied up in the particles. Given that the extinction data argue for dust being underabundant in the zone immediately in front of the MIF, the only easy way out is to argue that the grains have selectively been removed from the ionized gas. Ferland (2001) says that this is a process that must be operating if one is to have material flowing away from the MIF. However, an alternative explanation is that the grains near the MIF are modified by the ionized gas and/or the stellar radiation field.

3.3.3. THE EFFECTS OF SCATTERED EMISSION LINES ON SPECTROPHOTOMETRY In contrast to the situation of voiding some previous theoretical papers, where several detailed calculations of the incorrect model leave the results without an immediate application, a modern analysis of models of scattered emission line radiation is a potentially important, yet an incompletely studied subject. In their polarimetric study Leroy & Le Borgne (1987) pointed out that about 15% of the total observed [O III] 5007 Å radiation was scattered light. Observations of [S III], [O III], and [O II] emission lines are often accompanied by a slightly redshifted, broad and

weak "echo," which O'Dell et al. (1992) argue is light scattered from dust particles in or near the PDR. The redshift arises from the light being scattered by particles that are redshifted with respect to the emitting layer (the Doppler shift of the scattered light being doubled to an observer in our direction). The broadening arises from photons originating in an extended layer being scattered from an extended scattering layer. Hence a variety of redshifts are encountered at various angles. This interpretation was supported by Henney (1994) and the effects of plane-parallel slab scattering was calculated (Henney 1998). The existence of such an effect should have been anticipated since the adoption of the blister model for M 42 because we know from the scattered continuum that the PDR is an effective mirror. This effect may be more than an interesting artifact of the presence of dust, because the fraction of the emission line that is scattered light will be dependent upon the separation of the emitting and scattering layers and the wavelength dependence of the scattering and absorption properties of the particles. This means that emission line flux ratios that are not corrected for their scattering component will have an intrinsic uncertainty, even for the most spectrophotometrically accurate results. Fortunately, this uncertainty will be small as compared with the 15–20% fraction of the radiation that is characteristically scattered.

3.4. Characterization of Emission Line Velocities

The early papers on the blister model for M 42 (Balick et al. 1974, Zuckerman 1973, Pankonin et al. 1979) demonstrated the power of knowledge of the radial velocity of the emission lines for determining the structure of the nebula. This is certainly the case in the Huygens region because the MIF is viewed nearly face-on, and the emission is dominated by a single ionized layer. Things may not be so favorable when trying to use velocity data on the large scale (several parsecs), where the structure is probably more complex. In any event, one needs velocities at velocity resolutions of a fraction of the sound velocity, since this is about the velocity difference expected from motion away from an ionization front and at a spatial resolution small compared with the structure being modeled.

In terms of modeling the larger M 42 region a potentially useful data set over a $20'$ diameter (2.6 pc) with a spatial resolution of about $1'$ was derived by Hänel (1987) in Hα, [N II], [S II], and [O III], but a detailed model was not derived. A similar set of data was report by Seema (1996) for [O III] at much higher spatial resolution, but a detailed presentation of the data has not been made. Wilson et al. (1997) covered the inner $5' \times 5'$ field at $42''$ resolution in hydrogen 64α and combined that data with surface brightness information to model the MIF, producing the best picture of structure behind the Dark Bay. The complexities of trying to derive large scale models from emission line studies is demonstrated in the study of Goudis et al. (1984) who saw important secondary highly redshifted components extending over large areas.

3.4.1. RADIAL VELOCITIES IN THE HUYGENS REGION It is the Huygens region, because of its much higher surface brightness, that is easiest to observe and has been the subject of the most useful investigations. These studies have mostly been done

with slit spectroscopy. This has less inherent sensitivity than Fabry-Perot investigations but has advantages in terms of image processing and recognition of multiple velocity components. Even in this brightest region the perfect data set does not exist. By "perfect data set" I mean a set of slit spectra taken at intervals of no more $1''$, with a digital detector of high dynamic range, including emission lines covering the full ionization range and covering the full dynamic range of emission features. However, several data sets including some of these features do exist. Wilson et al. (1959) mapped the inner $4' \times 4'$ at $1.3''$ intervals in [O III], Hγ, and [O II] with the Palomar 5-m's coude spectrograph and photographic plates. Velocity images based on these data were later prepared by Fischel & Feibelman (1973) from the [O II] and [O III] lines. Modern CCD detectors were later used with the Kitt Peak National Observatory Coudé Feed Telescope's powerful spectrograph to map this same region. These studies offered incomplete spatial coverage owing to use of single slits (the Palomar study used multi-slits, at the expense of information about very high velocity components), but did include sampling of most of the region, with a high dynamic range, and over several hundred km s^{-1} velocity intervals. The Kitt Peak studies included [O III] (Castañeda 1988), [O I] (O'Dell & Wen 1992), [S III] (Wen & O'Dell 1993), [O II] (Jones 1992), H12 (Jones 1992), and Hα (Hu 1996a). The entire Huygens region has been covered in [O III] and [S II] (O'Dell et al. 1997) using a Fabry-Perot system at a velocity resolution of about 50 km s^{-1}, which is adequate for study of high velocity features. At the other extreme, Baldwin et al. (2000) have measured velocities of weaker lines and over a greater variety of ionization samples, but at only a single slit position.

This plethora of radio and optical high velocity resolution data allow one to draw some general conclusions. The central $2.5'$ diameter shows an almost constant [O I] velocity of about 25.5 km s^{-1}, whereas [O II] has a central value of 19 km s^{-1}, which becomes a few km s^{-1} bluer to the SW of θ^1. [O III] has a central value of about 20 km s^{-1}, the velocity becoming more blueshifted with increasing distance from θ^1 Ori C, with a local asymmetry of even greater values to the SW, a feature well defined in the 64α data. Given the fact that the foreground veil column density becomes less to the SW from θ^1 Ori C, the usual interpretation is that material is escaping the confinement of the veil material in that area and this is where the photoevaporative flow from the MIF leaves M 42. The radially increasing blueshift away from θ^1 Ori C is the opposite of what one expects for the concave model derived from the nebula's surface brightness. This is probably due to material near the sub-stellar point being subject to the most intense force due to radiation pressure and the stellar wind of θ^1 Ori C. The 64α velocities abruptly become more positive by about 7 km s^{-1} $3'$ east of θ^1 Ori C, which Wilson et al. (1997) correctly argue is probably where the MIF curves upward towards the veil material, thus removing the component of velocity due to expansion away from the MIF.

3.4.2. TURBULENT MOTIONS IN THE HUYGENS REGION It is for investigation of the fine scale motion that the finest-scale velocity studies of the main emitting layer have found their greatest application. These investigations have been phrased in

terms of study of the fine scale turbulence that occurs, a process initiated by Münch (1958). The modern method of statistical analysis has been through use of the structure-function (SF), $B(\phi)$, which is defined by $B(\phi) = \langle |V(\phi') - V(\phi'')|^2 \rangle$ where ϕ refers to the angular separation of two samples located at positions ϕ' and ϕ'', $V(\phi)$ is the observed radial velocity along a particular line of site, and $B(\phi)$ is calculated for all combinations of velocity samples. von Hörner (1951) has derived the expected properties of the SF for the case of a homogenous slab of emitting material and where the relative velocity, v, of two elements of the gas separated by a distance r varies as $v^2 \propto r^n$. For the common case of Kolmogorov turbulence, $n = 2/3$. When the sample separations are small as compared with the emitting layer thickness, $B(\phi) \propto \phi^{n+1}$ and when the separations are much larger than the layer thickness, $B(\phi) \propto \phi^n$. The transition between the two power laws is continuous and occurs at about the layer thickness.

This type of analysis has been applied to the CCD slit spectra. [O II], [S III], and [O III] all showed the property of a steep slope at small separation values, which then decreased at large separations. [O II] and [S III], which should both arise primarily from the He^o zone, behaved very similarly, with B increasing with a slope near unity at small separations and being essentially constant at large separations, with the transition occuring at about 22″. [O III] transitioned from a slope of 0.8 to ∼0.3 at about 15″. The average transition value, 18″, corresponds to a linear dimension of 0.04 pc. This is very close to the scale height for the density decrease in the flow away from the MIF. This can be argued to be a confirmation of the operation of the basic process of turbulence, although certainly not for confirmation of Kolmogorov turbulence with energies being fed in at a single scale size (an assumption in Kolmogorov's theory). The basic process is confirmed by the quite different behavior of the [O I] emission, which has an essentially constant slope of 0.7 ± 0.1 over the entire range of separations. Since the emitting zone thickness for [O I] should be $<1''$, this is the expected behavior, as the observed separations were all much greater than the thickness of the emitting layer for that line. Therefore, we see that the statistical analyses of the observed radial velocities through use of SF resemble the predictions of von Hörner's model for turbulence, although they do not match it exactly.

3.4.3. AN UNEXPLAINED RANDOM VELOCITY COMPONENT There is an additional puzzle that is revealed by high resolution spectroscopy. The lines are broader than expected from thermal broadening at the established electron temperatures. All of the CCD slit spectroscopy programs used for studying turbulence found that, after quadratically subtracting the observed linewidth (usually working in terms of FWHM, the full width at half of maximum intensity) for the instrumental and thermal broadening, all the ions showed a residual FWHM of about 9 km s^{-1}. The same result was found for the hydrogen 63α emission by Wilson et al. (1997), and is present, usually without recognition, in all previous high velocity resolution studies of M 42. The earliest indication seems to be in the Fabry-Perot study of Buisson et al.(1914). In that period before the identification of collisionally excited forbidden lines, Buisson et al. measured linewidths for the hydrogen and nebulium

lines, using the latter for determining the electron temperature, since FWHM = $0.214T_e^{1/2}/M^{1/2}$ when M is the mass of the emitting atom in atomic mass units (AMU). They obtained $T_e \simeq 15000$ K, and from that derived M(nebulium) $\simeq 2.7$ AMU, whereas the correct value is $\sim$16 AMU. The overestimate of T_e and corresponding underestimate of M reflects the role of the noninstrumental, nonthermal broadening of all the lines observed. The extra line broadening seems to be indistinquishably the same for ions of various mass and arising from quite different ionization zones, which argues that it is due to a gross motion. This suggests an origin of unresolved turbulence. However, the turbulent broadening expected from the best fitting models is about 2 km s^{-1} for the higher states of ionization and much lower for [O I].

This extra broadening cannot be overlooked. It means that as much energy is being carried by the nebular gas in this form of bulk motion as in thermal kinetic energy, therefore, the process could be of fundamental importance. What will determine that importance will be the timescale over which the energy is dissipated, i.e., the power it carries, rather than simply its energy. One knows that the processes of photoionization followed by recombination and collisional cooling cause the thermal gas to respond with a time constant of about $10^5/n_e$ years. Hence, a dissipation time for the unknown component that is much slower than this would mean that the process is secondary to the energy equilibrium of the nebula. The opposite is equally true. There is the possibility that the extra line broadening is due to the preferential blueshifted emission of material expanding away from the MIF, but the similar width of ions formed over a wide range of ionization zones argues against that. Henney (1998) has argued that this nonthermal broadening could be due to scattering by the dust in the foreground veil, but this is probably not the explanation since much of the scattered radiation will come from along the line of sight, where there would be no net velocity change of the radiation and the velocities differences between the emitting layers and the veil are not very great.

3.5. Magnetic Fields in the Region

Magnetic fields in H II regions have essentially been ignored as being unimportant or (worse) untreatable in considering the processes that determine the physics. It is impossible at present to make a direct observational determination of the strength (B) with an H II region; but, one can make oblique arguments for their presence. Certainly such fields are ubiquitous throughout the interstellar medium and within molecular clouds. Within the imbedded star formation region near the BN-KL sources to the NW from the Trapezium the field has been measured by Zeeman splitting of emission lines (Crutcher et al. 1999). Since this region is likely to be quite different from M 42, it is unwise to use this for information about the H II region. However, the magnetic field strength has been determined (Troland et al. 1989) in the foreground veil material from Zeeman splitting of the H I 21-cm line seen in absorption in the background nebular radio continuum. This study was done at a spatial resolution of 40″ and showed that there is a strong correlation with extinction, so that the field lies within the veil material. The measured peak

values are typically B = 200 μG, which would mean total strengths of 400 μG if the field is isotropic. This value is at least an order of magnitude above that in the general interstellar medium and indicates that the field was frozen into the contracting parent GMC. This means that the energy density of the magnetic field in the veil is about 5×10^7 K cm^{-3}, which is comparable with the thermal energy (9×10^7 K cm^{-3}) near the MIF (Ferland 2001).

The closest thing one has to a direct determination of B is from the Faraday rotation measure (RM) of the CN emission arising from the BN-KL source. Rao et al. (1998) determined that RM $< 2.8 \times 10^4$ rad m^{-2}, which gives $\int N_e \, dl = 0.035$ G cm^{-3} pc. In this region, n_e at the MIF is about 2×10^3 cm^{-3} (Pogge et al. 1992). Using the exponential density drop model and an emitting layer equivalent thickness of 0.1 pc gives B < 350 μG. Rao et al. derive a ten times smaller upper limit through adopting a 1 pc emission layer thickness. The uncertainty of the RM is ill determined, so that the resultant upper limit to B shares this uncertainty. Determination of an accurate RM in M 42 is extremely important.

It may be that the nonthermal optical line broadening is evidence for a magnetic field in the main emitting layer of M 42. Magnetic fields allow the formation of Alfvén waves of velocity $v_A^2 = B^2/4\pi\rho \simeq 7.5 \times 10^5/n_e$, where ρ is the mass density gm cm^{-3} and n_e the electron density (cm^{-3}) (Spitzer 1978, Ferland 2001). Alfvén waves are certainly present in GMC where the highly supersonic line broadening of the molecular emission is best explained by them (Myers & Goodman 1988). If there is a magnetic field in the main emitting layer, the Alfvén wave velocity would be about 9 B_{400} $n_4^{-1/2}$ km s^{-1}, where B_{400} is the magnetic field in units of 400 μG and n_4 is the electron density in units of 10^4 cm^{-3}. This means that Alfvén waves would have velocities comparable to the nonthermal line broadening that is observed. Although an attractive idea, explanation in this fashion would require that the field strength increases with decreasing n_e, a counter-intuitive result, in order for the extra line broadening to be the same for all ions. If Alfvén waves of this strength are present, their energy density (Ferland 2001) would be about 5×10^7 K cm^{-3}, i.e., about half that of the thermal energy. The importance of such magnetohydrodynamic waves in the power balance of the nebula is uncertain. The timescale for dissipation of Alfvénic waves is quite uncertain so we do not know if this energy is important to the power balance. The fact that the FWHM broadening attributed to the putative Alfvénic waves (9 km s^{-1}) is less than the sound speed of 17 km s^{-1}, argues that Alfvénic driven shocks are not being formed and that the dissipation rate is low.

4. THE ORION NEBULA CLUSTER

The eponymous cluster of stars associated with M 42 (the Orion Nebula Cluster, ONC) reveals itself most clearly in infrared images because most of the members are of low surface temperature. Figure 7 gives a recent depiction in the JHK bandpasses. The cluster's appearance is dominated by the bright O and early B stars of the Trapezium (common name θ^1 and designated A through D

progressing from west to east, then jumping back to E, which is located 4″ north of θ^1 Ori A) and the θ^2 stars. The lower luminosity stars appear clustered about a center near the Trapezium, and the total membership of the cluster is about 3500 stars and a cluster mass of 1800 $M_\odot$ (Jones & Walker 1988, Hillenbrand & Hartmann 1998). This is to be compared with the approximate 2 $M_\odot$ of ionized gas near the MIF (Wilson et al. 1997) and the OMC-1 mass of about 500 $M_\odot$ (Evans et al. 1975). ONC is the densest nearby star cluster, having a central density of about 2×10^4 stars pc^{-3} (Hillenbrand & Hartmann 1998).

4.1. ONC Membership, Internal Motion, and Structure

Fortunately, because of the high galactic latitude ($b = -19^\circ$), proximity, and location on the near side of the obscuring cloud OMC-1, most of the stars that appear associated with the ONC, are. This result is confirmed by the proper motion studies of the region, the most definitive investigations being of the brighter stars by van Altena et al. (1988) and the fainter members by Jones & Walker (1988). Neither of these studies demonstrated the cluster expansion that was reported by Strand (1958), which argued for a time of origin of the expansion of about 3×10^5 years. Unfortunately, the brightness of the Trapezium stars renders it impossible to accurately put them into the reference frame of motion of the remainder of the cluster, a situation not remedied by Hipparchos observations because of the complexity of the field. With its superior proper motion errrors (± 0.15 mas/yr) the van Altena et al. (1988) study provides the best guide to internal motions. These authors found a value of 0.70 ± 0.06 mas/yr, which at 450 pc distance corresponds to an internal velocity dispersion of 1.5 ± 0.1 km s^{-1}. Perhaps surprisingly, the most useful observations of motions within the Trapzium itself come from visual observations dating back to the 1830s (Allen et al. 1974), which show no relative motion of the brightest four stars within an accuracy of about 1.5 mas/yr, with only the E component showing a noticeable relative motion (away from component A) at 2.2 mas/yr, although this measurement would have been the most difficult in which to avoid long term errors. There is a suggestion that the velocity dispersion varies with the stellar mass. The van Altena et al. study sampled more massive stars and found a smaller velocity disperson than the Jones & Walker study of less massive stars, a trend similar to that seen by Walker (1983) in radial velocities of stars over spectral types B-K.

Hillenbrand & Hartmann demonstrate that the distribution of all the member stars resembles that of a single mass King-Mitche cluster model (thus resembling a gravitationally relaxed system in dynamic equilibrium), but point out that the total stellar mass required to produce gravitational equilibrium is about twice that derived from the stellar census. There seems to be a concentration of high mass stars towards the center of the cluster. This distribution of members and mass segregation is usually indicative of a relaxed stellar system, but this cannot be the case because the young age of the cluster (next section) of less than 10^6 years means that there has not been enough time for relaxation to occur. A star moving at 0.7 mas/yr could have crossed the central core of 85″ no more than eight times.

This caused Hillenbrand & Hartmann to conclude that the more massive stars formed in what was originally a high density core. These authors do not address the anomalous location of the massive θ^2 stars far outside the central core of the cluster.

The dynamical effects of this rich very young cluster is considered in detail by Bonnell & Kroupa (1998) and Kroupa (2000). The dynamical evolution of the stars is rendered quite complex since the photoionization of the surrounding gas has probably led to the photoevaporation of a significant amount of mass. The present mass loss rate is about $2 \times 10^{-4}\ M_\odot\ yr^{-1}$ (the ionized mass divided by the time for an element of material to cross the 0.1 pc thickness of the nebula), which means that a significant fraction of the total mass can have been removed in 10^6 yrs. As shown in Section 7.4, there is evidence that the ONC is only one of three regions of recent massive star formation, the others remaining imbedded in OMC-1.

4.2. Age, Initial Mass Function, and Binarity within the ONC

The youth of the ONC is obvious from the fact that it contains O stars still on the main sequence, but an accurate assessment of the age requires a detailed knowledge of the lower mass objects. This is because the most massive stars collapse to the main sequence very rapidly and their lifetime on the main sequence can exceed the age of the cluster. The collapse of lower mass protostars occurs more slowly, so that one catches them in their pre-main sequence stages, thus allowing chronology to be performed. Lower mass protostars collapse more slowly, which means that a cluster with a single epoch for onset of star formation would have its stars spread out along a single line along the upper main sequence (where the protostars have reached their initial equilibrium hydrogen burning state but not yet exhausted that fuel source), then trailing off above the main sequence in the Hertzsprung-Russell (H-R) diagram (or its photometric equivalent) in a single line that serves as a unique age indicator. In the real world things are not this clear. There may be a spread of protostar ages, there will be spectral classification uncertainties and photometric uncertainties both observational and in the amount of the interstellar extinction correction, and the protostar models are sensitive to the allowable range of parameters assumed in their calculation.

The earliest definitive work on the H-R diagram is the spectroscopic study of Walker (1983), which was soon followed by a primarily photometric study by Herbig & Terndrup (1986) who established the age as being about 10^6 years and that the cluster was unusually dense. The scattered light in the visible makes it difficult to obtain good photometry of the fainter members, so the study of the photometric H-R diagram benefitted by the improved angular resolution of the Hubble Space Telescope (HST) (Prosser et al. 1994). The most comprehensive study is that of Hillenbrand (1997) who combined spectroscopy with photometry extending to the diagnostically more sensitive infrared I bandpass. Her Figure 13 shows her observations, with the protostar tracks and isochrones being those of D'Antona & Mazzitelli (1994). The diagram demonstrates the fact that the age of the cluster is

small (less than 10^6 years) but that there is not a good fit to a single age. As we will see in Section 6.3, most of the stars have significant circumstellar disks of material, so the extinction corrections are difficult to determine and introduce an uncertain magnitude of scatter in this diagram. Hildebrand also points out the sensitivity of the protostar models, comparing her observations with the models of Swenson et al. (1994). Palla & Stahler (1999) have compared her observations with their most recent set of protostar models and conclude that the best fitting single age is 2×10^6 years, but that star formation began at a low level about 10^7 years and has accelerated to the present. Hillenbrand & Carpenter (2000) extended the photometry to include the redder H(1.6 μm) and K(2.2 μm) bandpasses, compared the results with updated D'Antona & Mazzitelli (1997) models, and found assumed age distributions that are uniform in logarithm between 10^5 and 10^6 years to be indistinguishable from one uniform in logarithm between 3×10^4 and 3×10^6 years, and that both closely resemble the derived distribution of stellar ages. Luhman et al. (2000) compared their HST near infrared observations and groundbased K band spectra with the newer D'Antona & Mazzitelli (1997) models and found a median age of 0.4×10^6 years.

In terms of the distribution of stars of different mass there are two issues. They are 1. agreement of the distribution with the well established Initial Mass Function (IMF) (essentially the question of whether or not this is universal), and 2. the behavior of the function at the lowest masses (which is difficult to determine in field stars and is germaine to the question of the formation of brown dwarfs and even free-floating planets). Both Hillenbrand & Carpenter (2000) and Luhman et al. (2000) find an IMF in agreement with the commonly adopted values, although Hillenbrand & Carpenter find evidence for an excess of more massive stars in the central core of the ONC. Both investigations show a peak IMF at 0.15 $M_\odot$, with the former finding a drop of 0.55 dex and the latter 0.35 dex at 0.025 $M_\odot$. Since brown dwarfs are usually identified as stars of less than 0.08 $M_\odot$, the ONC is the most abundant sample of these objects. Recent IHK observations to very faint limits (Lucas & Roche 2000) find several objects below the deuterium-burning (planetary) threshold of 0.013 $M_\odot$, which they identify as free-floating planets, i.e., planets not gravitationally attached to a specific star. This result is disputed by Hillenbrand & Carpenter, who argue that the effects of field star contamination and the uncertainties in the collapsing object models make this claim unreliable. Infrared spectroscopy of the candidate substellar objects supports that identification (Lucas et al. 2001). Similar claims of discovery of isolated planetary mass objects have also been made for the σ Ori cluster (Zapatero Osorio et al. 2000).

A final question of broad import is the fact that the fraction of binary stars in the ONC (Padgett et al. 1997, Petr et al. 1998) is in agreement with nearby field stars and less frequent than in the Taurus-Auriga low density star formation region. Kroupa et al. (1999) argue that this reflects the realities of gravitational interactions of both the cluster stars and the surrounding gas mass. If this reasoning is correct, it establishes that initial binarity is common, but decreases rapidly in the rich clusters that are thought to dominate in eventually populating the field stars in our Galaxy.

5. PROPERTIES OF THE STARS

The characteristics of θ^1 Ori C determine most of the properties of the photoionized material we see as M 42. This means that the properties of the star are important for the nebula and for the questions of continued star birth and survival of the circumstellar clouds around the low mass young stars. In addition, the group properties of the other stars contain useful information about the process of star formation.

θ^1 Ori C is a characteristically peculiar O6 star (Walborn & Panek 1984) that has a strong stellar wind. However, it is unusual in that it manifests a 15.4 day periodicity in spectra (Walborn 1981, Walborn & Nichols 1994, Stahl et al. 1993, 1996) and X-ray emission (Gagnè et al. 1997). Well sampled searches for periodicities in its radial velocity indicate no associated pattern (Stahl et al. 1993). Most germaine to the structure of the nebula is the spatial motion of this star. Because of its brightness and the complexity of the field, good proper motions do not exist. The star has been the subject of numerous radial velocity determinations during the twentieth century (summarized in O'Dell 2001a). The commonly cited values are probably too large. Conti (1972) found $V_r = 26 \pm 3$ km s^{-1}, whereas Stahl et al. (1993) found $V_r = 14 \pm 1$ km s^{-1} with a brief period of significantly smaller velocity. At about the same time (1993) O'Dell & Brown (O'Dell 2001a) found $V_r = 14 \pm 1$ km s^{-1}. If these recent values are representative of the mass motion of the star, then it is moving away from OMC-1 at 14 km s^{-1} and would cover the distance from the present position of the MIF in only 1.8×10^4 yrs, causing significant changes in the nebula and the illumination environment of the low mass stars and their disks. However, such a high velocity with respect to the parent cloud and the remaining stars (similar values) is difficult to accept, especially in light of the known outflow from the star and its variable atmosphere. In Section 4.1 we saw that there was no evidence for a large peculiar motion of θ^1 Ori C in the plane of the sky.

The stellar rotational velocities of the ONC stars differs significantly from the Taurus stars, indicating either different conditions of formation or, in the subsequent pre-main sequence, evolution. The cause of the difference is probably due to the age or environment of the regions because one expects most young stars to be confronting the problem of having the maximum angular momentum that would still allow formation. The angular momentum problem is exacerbated by continued accretion of material onto the star from their inner circumstellar disks. The ONC stars exist with rotation velocities near the breakup velocity (Clarke & Bouvier 2000), which is not the case for the Taurus stars. These conclusions are drawn from both spectroscopic measurement of the Doppler broadened linewidths (Stassun et al. 1999) and determination of rotation periods from photometrically monitoring the stars (Herbst et al. 2000). The common wisdom is that the inner disk material serves as a brake for stellar rotation. However, one cannot invoke the absence of a brake to explain the ONC properties since there is no evidence for destruction of the disks. The remaining important difference is the youth of ONC.

The abundances in the ONC region fit into well defined global patterns. The lithium abundances are high (Duncan & Rebull 1996), but the trend seen in the

much older Pleiades cluster (more rapidly rotating stars have greater lithium abundances) is absent. There are interesting abundance differences in member stars of the larger Orion associations (Cunha et al. 1998), but no specific information on the small sample of stars in the core of ONC.

The ONC stars were among the first discreet X-ray sources detected, and rapidly improved observations have revealed that both the O-B main sequence stars and many of the pre-main sequence stars are luminous X-ray sources. The magnetically driven emission mechanisms for the low mass stars are described by Feigelson & Montmerle (1999) and it is argued (Caillault & Gagnè 1994) that the emission from the early type stars arises in unseen low-mass binary companions, although θ^1 Ori C is the brightest X-ray source in the region (Schulz et al. 2001) and its spectrum is well modeled by an extended atmosphere of 5×10^6 K (Geier et al. 1995). The particular advantage of X-ray observations is the low opacity of the OMC-1 material, which allows study of not only the ONC members that lie beyond the MIF, but also stars in the secondary star formation regions near the BN-KL source. The power of the approach is demonstrated by the fact that the Chandra Observatory has led to the detection of about 1000 X-ray sources in this area (Garmire et al. 2000).

6. THE PROPLYDS

Arguably the most rapidly advancing area of Galactic astronomy is star formation, a subject exploiting the rapid growth of infrared and millimeter observational capabilities. At the same time, optical studies with increasing spectral resolution and time coverage have produced remarkably detailed knowledge about young stellar objects (YSO's) once they are sufficiently free of their circumstellar clouds to be visible. In M 42 one sees YSO's in a nontraditional environment for this area of study, so that the selection effects in detecting and studying the objects are quite different from normal practice. Moreover, the YSO's are subject to processes that strongly affect their structure, through the intense ultraviolet radiation field and close gravitational interactions, and possibly their continued existence. These important factors, peculiar to M 42 and similar regions, has lead O'Dell & Wen (1994) to designate YSO's found in or near H II regions as "proplyds." The word appears to be a contraction of protoplanetary disk, which the objects may or may not include, but it is only a name, in the same way that quasar originated as a convenient contraction of quasistellar radio source. This section reviews our present understanding of the proplyds and what this says about the universal process of star and planet formation. As we will see, the characteristics that define the subclass of YSO's that are proplyds are important in determining whether or not their circumstellar disks will survive.

The recognition of the special status of the proplyds began gradually, since they appear stellar in typical groundbased telescopes. Laques & Vidal (1979) were the first to identify them as peculiar objects when they found six stars near

θ^1 Ori C to be high ionization emission line sources. The next big step was the application of VLA resolution of about 0.1″ to the inner M 42 region, where it was found (Churchwell et al. 1987, Garay et al. 1987) that these (and some two dozen additional objects) were photoionized gases, and in a subsequent study (Felli et al. 1993) it was determined that one could resolve a bright cusp structure on the side of the objects facing θ^1 Ori C, arguing that these were compact neutral clouds photoionized by θ^1 Ori C. At this point one could not clearly say what the objects were, although Churchwell did identify the correct model as a likely possibility, as did Meaburn (1988). It was, however, the quantum step in angular resolution allowed by the HST that allowed a clear delineation of their true nature (O'Dell et al. 1993) because one could now see that many of the stars in the ONC were actually extended emission line sources and that some objects are seen as dark silhouettes.

6.1. HST Observations of the Proplyds

Characteristically the objects' bright cusps face θ^1 Ori C, although as one searches to the SE, the structures become more uniformly illuminated and some of the distant objects are oriented towards the O9.5 V star θ^2 Ori A (O'Dell et al. 1993). When one takes into account the line-of-sight projection effects, the distribution of forms indicates that the physically closest proplyds to θ^1 Ori C have the most elongated forms. This variation must be due to either the stellar wind from θ^1 Ori C or the effects of radiation pressure (O'Dell & Wen 1994). At the other end of appearance are the silhouette objects, which show no evidence of local photoionization and they are seen in extinction against the bright background of the MIF. A sample of four of the 150 known proplyds (O'Dell & Beckwith 1997) is shown in Figure 8, where it is illustrated that many of the bright edged proplyds also have a visible dark disk near the central star. At this time there are 15 known pure silhouette proplyds, and the central star is visible in all except two. Because objects continue to be found, a designation system based on coordinate boxes (1″ in Declination, 1.5″ in Right Ascension) is now used (O'Dell & Wen 1994). As an example, the object located at 5:35:17.67 −5:23:41.0 (2000) is designated as 177–341.

6.2. The Basic Model

One basic model explains the various appearances. The pre-main sequence stars are all surrounded by a circumstellar disk that is concentrated in density to the equatorial plane and the inner regions of the disk. It takes little neutral material to produce an ionization boundary, so that a local ionization front is formed in the outer parts of the circumstellar cloud. For those objects shielded from photoionization by θ^1 Ori C by being located within the foreground veil of neutral material, no local ionization boundary is formed and the objects are seen in silhouette. The dominant source of photoionization by θ^1 Ori C is confirmed not only by the orientation of the ionized cusps, but also by the observed dependence of the

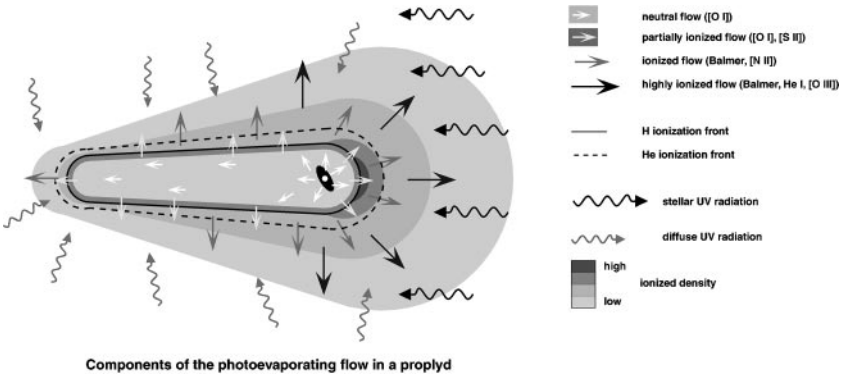

Figure 9 The most satisfactory model for the bright-rimmed proplyds involves heating an inner molecular disk by <13.4 eV photons, producing a slow neutral wind of gas, in which a local ionization front is formed. Material in the ionized zone expands rapidly (Henney & O'Dell 1999).

surface brightness upon distance from θ^1 Ori C (McCullough et al. 1995, O'Dell 1998a). The various forms and visibilities of the inner disks are determined by their apparent random orientation.

The corresponding physical model is shown in Figure 9 (Henney & O'Dell 1999), which is derived from the work of Henney & Arthur (1998), and Johnstone et al. (1998). The local ionization front is formed where photons of $\geq$13.4 eV are completely absorbed. The density at this front (for the innermost proplyds) is about 10^{5-6} cm^{-3}. Because this density is much greater than the ambient nebular gas, the ionized gas freely expands, in the same way that material flows away from the MIF. The gas in the inner disk is molecular and is heated by photons of <13.4 eV, photodissociated and heated, and producing a slow wind of neutral atomic gas expanding outwards. One sees a striking confirmation of this model in the direct detection of H_2 emission from the inner disk (Chen et al. 1998) and also in the distribution of [O I] emission. In 182–413 one sees [O I] emission surrounding the inner disk in addition to that in the local ionization front, which should not be possible from the process of photoionization and collisional excitation. Störzer & Hollenbach (1998) demonstrate that this inner [O I] emission can arise from photodissociation of OH molecules that leave OI in the necessary excited state.

6.3. How Common are the Circumstellar Disks, and How Long will they Survive?

Almost all stars in the ONC have detectable circumstellar material. Within the proplyds there are two selection effects. The bright cusp proplyds are quite visible when they are physically close to θ^1 Ori C because of the inverse square dependence of their surface brightness, which means that if there is sufficient material to

form a local ionization front, the object will be bright. O'Dell & Wong (1996) show that within a projected distance of 30″ from θ^1 Ori C, 66% of all stars are proplyds. When one considers the projection effects (some of these objects will be more distant and only appear close), the frequency must be higher. The conditions necessary to detect a silhouette proplyd are more demanding, requiring higher signal to noise in the image, location outside of the ionized gas zone, and sufficient mass and distribution of the material (Bally et al. 2000). These conditions mean that the fraction of ONC stars belonging to this class is not really useful in estimating frequency of circumstellar material. Direct detection of thermal radiation at the shorter infrared wavelengths (which selectively detects the hottest inner portions of a circumstellar disk) has lead Hillenbrand et al. (1998) to conclude that the frequency of circumstellar disks is at least 55%, and probably no more than 90%. A similar study that includes their own L band observations led Lada et al. (2000) to estimate the frequency as 85%, and within the proplyds it is 97%. The latter number indicates that having an outer gaseous envelope is always accompanied by there being an inner circumstellar disk.

The same PI process that renders the bright proplyds so visible also threatens their survival. As explained in the preceding section, the photoionized material is expected to rapidly flow away from the local ionization front. Drawing on basic considerations and model calculations when the proplyds were thought to be simple partially ionized globules, Churchwell et al. (1987) pointed out that if their masses were like those of typical YSO's, the circumstellar material would be lost on a timescale short compared with the lifetime of θ^1 Ori C. There have been several studies that have modeled the proplyds and estimated their mass loss rates (e.g., Johnstone et al. 1998, Henney & Arthur 1998, Störzer & Hollenbach 1999). However, in principle one can diminish the dependence of the assumptions of the model by making direct observations of the gas streaming off the proplyds. An initial attempt at this was made by Henney et al. (1997) using Massey & Meaburn's (1995) spectroscopic data set, but the contrast of the proplyd spectra against the nebular emission in the same line and at similar velocities made the result uncertain. The best ground-based study is the recent Keck study (Henney & O'Dell 1999), which shows that the mass loss rates are about 0.4×10^{-6} $M_\odot$ yr^{-1} with an uncertainty of 50%.

Survival of the bright proplyds then depends upon the mass of the reservoir of material present, which is difficult to determine. At present, only estimations based on far infrared and millimeter thermal emission exist (Bally et al. 1998b, Mundy et al. 1995, Lada et al. 1996), a difficult task because of the bright and variable background from the nebula and PDR. Under the assumption that the observed emission from the dust component can be scaled to a total mass using the interstellar gas to dust mass ratio of about 100, the most massive circumstellar clouds are ≤ 0.015 $M_\odot$. Combined with the Henney & O'Dell mass-loss rate, this means survival for only 4×10^4 yrs.

The existence of the proplyds in the face of such a short timescale presents a basic conundrum. Are the methods of calculating total masses flawed? Is θ^1 Oric an extremely young star? Are the stars in highly elliptical orbits? If the dust

particles in these YSO's have already been selectively accreting into large bodies, then the thermal emission estimates will be much lower than the true mass. This might be the case because the derived masses in the ONC are fully an order of magnitude less than usually derived for YSO's. To be sure, there is a range of ages of stars in the ONC. However, formation of θ^1 Ori C, immediately followed by rapid photoionization of the surrounding gas, would have stopped star formation. This means that one would expect θ^1 Ori C to be the youngest star in the visible ONC cluster. However, one must ask why we would be so lucky as to live in the brief period after the formation of θ^1 Ori C and the short time before the destruction of the circumstellar material around the other stars. Störzer & Hollenbach (1999) argue that the low mass stars of the ONC could be in highly elliptical orbits, thus ablating material only in the brief periods when near θ^1 Ori C, but this hypothesis is difficult to prove. Evidence for very great youth comes from the study of BM Ori (θ^1 Ori B) by Palla & Stahler (2001), who find that star to have an age of $<$100,000 years. The riddle of the existence of the proplyds remains. The riddle is one of great importance, because the rapid destruction of the circumstellar material in this rich young cluster would argue that planet formation is a rare event, reserved for stars formed in the less rich clusters where a massive ionizing star never appears.

Proplyds in M 42 are not unique, but rather, are simply easier to discover because of the proximity of the nebula. Similar objects have now been found in the giant cluster NGC 3603 (Brandner et al. 2000) and in M8 (Stecklum et al. 1998). Spectroscopic evidence exists for dense ionized knots, similar to the proplyds, near π Scorpii (Bertoldi & Jenkins 1992).

7. HIGH VELOCITY OUTFLOWS AND SHOCKS

There is a wealth of high velocity features seen in M 42. These include bipolar jet flows from low mass stars and shocks formed where these collimated flows interact with the ambient ionized gas of the nebula and the foreground veil of neutral material. In addition, there are uncollimated flows from both the low mass contracting stars and the more important stellar wind from θ^1 Ori C, both phenomena producing shocks. In addition to these processes clearly associated with ONC stars, there are imbedded sources of outflow in the BN-KL and Orion-S regions that produce features in M 42.

7.1. Bipolar Collimated Flows from Low Mass YSO's

Bipolar flow seems to be a natural part of the accretion phase of YSO's. This means that it has been no great surprise to discover that this phenomenon is common in the ONC, where 25 mono-polar or bipolar jets are seen (Bally et al. 2000, Bally & Reipurth 2001). These jets are difficult to identify because they are seen against the bright background emission in the same lines that are produced in the nebula. The ones seen in M 42 qualify to be called microjets since they have characteristic lengths of about 400 AU. The estimates of their momentum flux

characterizes them to be much less energetic than the flows driving the classical HH objects, which do not occur in photoionized regions. Spectra exist of a few of the objects (Bally et al. 2000), and the radial velocities are about 100 km s^{-1}. A low ionization microjet is shown in Figure 10. This object (244–440) has its jets confined to within its local ionization front and they appear best in [O I] emission. Microjets extending beyond the local front in other objects are of higher ionization because of photoionization by θ^1 Ori C. A majority of the microjets appear monopolar. The meaning of this property is not clear. It is most likely to be an observational or excitation selection effect because it is difficult to imagine intrinsically monopolar flows.

7.2. Large-Scale Flows and Shocks

In addition to the close-in bipolar flows one sees a few examples of extended jets, although no extended bipolar jets have been found. The largest of these are the highly blueshifted features seen in the Fabry-Perot study of O'Dell et al. (1997). These appear to drive the features known as HH 202 and HH 203 + 204. A quite different feature, initially discovered on the Fabry-Perot monovelocity images, is a highly structured filament that appears to drive the features designated as HH 529. All of these jets have associated shocks that must be the result of the jets impacting lower velocity ambient material. In addition, there are several systems of shocks, e.g., HH 269 and HH 528, where the causal jet has not been seen. The largest of these is HH 528 and one set (HH 513) is bipolar with a well defined proplyd in the middle. Fortunately, the time interval between HST observations is long enough that tangential motions corresponding to about 30 km s^{-1} can be detected, which helps to define the flows (Hu 1996b, Bally et al. 2000). The timescales derived by dividing the angular distances from the apparent sources by the tangential motions gives values from 100 to 1000 years, indicating that shocks driven by flows are a current feature of M 42. However, the largest values are not limits to the duration of the activity because shocks formed further from the sources may not be as visible.

The radial velocity values of the shocked material are primarily blueshifted, this being well defined for the HH 202 and HH 203 + 204 regions (O'Dell et al. 1997), which may be unrelated. However it is also true for HH 529 and HH 269, shown in Figure 11 to both appear to be part of a common bipolar flow. A selection effect obviously is occurring in the detection of the material shocked by bipolar jets. The shocks that are formed by blueshifted material occur in less dense material and are therefore more visible. The shocks from the redshifted jets occur in the main emitting layer where they have low contrast against the surrounding material. Some of the shocks have high ionization, being quite visible in [O III]. This indicates that they are formed in gas that has already been photoionized by θ^1 Ori C. However, blueshifted features like HH 202, HH 269, and HH 203 + 204 have strong low ionization components and relatively weak [O III]. It is most likely that these are features are being formed when the jets impinge on the neutral foreground veil material (O'Dell et al. 1997).

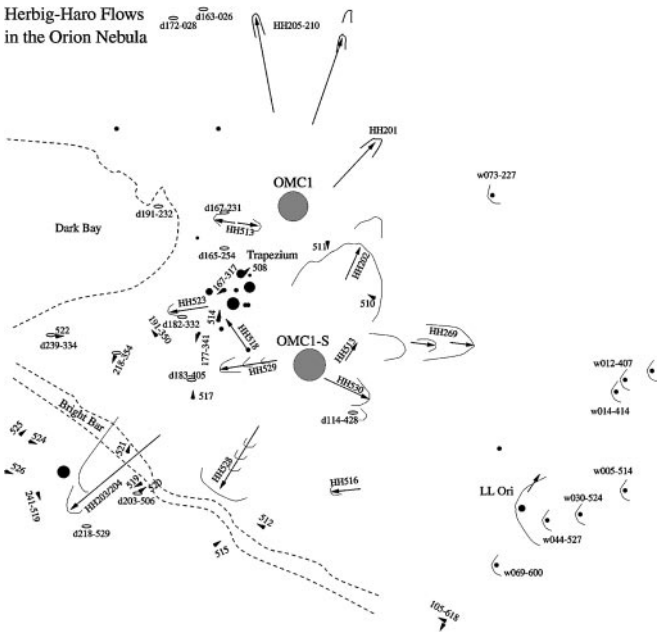

Figure 11 This cartoon (Bally et al. 2000) of M 42 depicts the location of the microjets (short arrows), large scale flows (arrows labeled with HH designations), wind driven shocks (w notations), and 12 of the 15 silhouette proplyds (d notations).

7.3. Stand-off Shocks

There are also two types of shocks that appear to be stationary. One set of shocks is limited to proplyds close to θ^1 Ori C (Bally et al. 1998a, 2000). Their position, and no detectable tangential motion, argues that these shocks form when the gas being photoevaporated from the proplyds shocks against the high velocity stellar wind from θ^1 Ori C. They are closely oriented to vectors that point from the proplyds to θ^1 Ori C and found within a distance of 15″. This must define the region in which the free flow of wind is occuring. These shocks are all high ionization, as expected if they are physically close to θ^1 Ori C. A related type of shock, also with no measured tangential motion, is found further from θ^1 Ori C. The best example of this type is the shock associated with the T-Tauri star LL Orionis. The photoionization will be less at the large distances where these shocks are found. They are low ionization features, and the effects of the wind from θ^1 Ori C are negligible. They do not show strict orientation towards θ^1 Ori C. Bally et al. intepret these as shocks formed when the noncollimated (but not photoevaporation driven) outflow from the YSO's shock against low density gas flowing away from the central region of M 42. In the case of the largest silhouette proplyd (114–426), which must lie within the veil material, one sees a shock probably caused by the general outflow shocking against the ambient neutral gas.

7.4. Outflow from the Two Imbedded Star Formation Regions Near BN-KL and Orion-S

There are two regions of infrared emission that must arise from early type stars imbedded sufficiently deep in OMC-1 as to be optically invisible. The more luminous of these is associated with the BN-KL region and the specific source IRc-2 and is the subject of important recent articles (Menten & Reid 1995, Rodríguez-Franco et al. 1999). The less luminous has received much less attention and is usually called the Orion-S region. Since the subject of the current review is the optical object M 42, I will only treat these objects as they are related to the nebula. The positions of both are indicated in Figure 11.

The BN-KL region has an associated set of optically discovered (Axon & Taylor 1984), rapidly moving (Jones & Walker 1985, Hu 1996a,b), knots of low ionization whose form and velocity distribution indicate that they are shocks. Allen & Burton (1993) found that there is a host of fingers of H_2 emission centered on BN-KL and that the tips of these fingers are bright in infrared [Fe II] emission. Most, but not all of the fingers have optical features at their tips, with increasingly sensitive infrared (McCaughrean & Mac Low 1997) and optical (O'Dell et al. 1997) studies keeping abreast in detections. The dynamic age of the tips is less than 1000 years. Burton and his colleagues refer to these features as "bullets," a vivid term that communicates well the idea that these are moving discrete masses. However, it is not obvious how such a wealth of projectiles could have exploded from a source near BN-KL. Stone et al. (1995) argue that the fingers could be Rayleigh-Taylor instabilities originating when an earlier slower stellar wind is overtaken by a later faster moving stellar wind. Certainly this mechanism can produce fingers of the observed form and kinematics (Tedds et al. 1999, Lee & Burton 2000), but it does not explain why most of the fingers have optically visible tips. That feature can be explained (O'Dell et al. 1997) if the instability is the result of a single stellar wind blowing into the decreasing density material near the surface of OMC-1. In any event, all of the evidence is for there being young luminous stars at the core of BN-KL and outflow from them is expected. There is no optical indication of this activity except for the tips of the Allen & Burton fingers.

The Orion-S region is most clearly delineated in the 1.3 mm thermal radiation of its dust (Mezger et al. 1990) where it is about one-tenth as bright as the BN-KL region. Unlike the northern source, where the surface of M 42 is smooth, Orion-S is located within a local rise (closer to the observer), which suggests that this source is closer to the surface of OMC-1. It also suggests that this is a region of higher molecular cloud density and that the main ionization front of M 42 has penetrated less far through the process of photoevaporation. There are two bipolar outflows seen in molecules. A high velocity flow (Rodríguez-Franco et al. 1999) of about $\pm$ 100 km s^{-1} is centered a few arcsec NE of the source FIR-4 and expells material to the NW (blueshift) and SE (redshift). A more extended low velocity $\pm$ 5 km s^{-1} bipolar flow is oriented NE (blueshift)-SW (redshift) and along a line passing within $2''$ of the FIR-4 source (Schmid-Burgk et al. 1990). There are

numerous optical flows that appear to originate from close to Orion-S (labeled OMC1-S in Figure 11), including HH 529, HH 269, and HH 530; however, the symmetry axes of HH 529 and HH 269 clearly lie to the north of the core of Orion-S which produces the bipolar molecular outflows (Bally et al. 2000). It is likely that the bipolar molecular outflows originate at or near a deeply imbedded luminous star, while the optical features are driven by low mass stars very near the surface of M 42. The best candidate for the source of the irregular jet that appears to drive HH 529 is object TPSC-1 (Lada et al. 2000), which is seen only in the L band.

ACKNOWLEDGMENTS

I am grateful to numerous colleagues with whom I've discussed M 42 over the last 40+ years, beginning with D. E. Osterbrock and most recently Reggie Dufour, Patrick Hartigan, Will Henney, and Gary Ferland. The last two colleagues made careful critical readings of the draft manuscript, although the judgments of the final version remain mine. Special thanks are owed my graduate students Hector Castañeda, Takao Doi, Xihai Hu, Michael Jones, Zheng Wen, and Shui-Kwan Wong who did much of the thankless work and contributed original ideas that have helped elaborate our knowledge of the optical nebula.

LITERATURE CITED

Allen C, Poveda A, Worley CE. 1974. *Rev. Mex. Astron.* 1:101–18

Allen DA, Burton MG. 1993. *Nature* 363:54–56

Axon DJ, Taylor K. 1984. *MNRAS* 207:241–61

Baade W, Minkowski RL. 1937. *Ap. J.* 86:119–22

Baldwin JA, Crotts A, Dufour RJ, Ferland GJ, Heathcote S, et al. 1996. *Ap. J.* 468:L115–18

Baldwin JA, Ferland GJ, Martin PG, Corbin MR, Cota SA, et al. 1991. *Ap. J.* 374:580–609

Baldwin JA, Verner EM, Verner DA, Ferland GJ, Martin PG, et al. 2000. *Ap. J. Suppl.* 129:229–46

Balick B, Gammon RH, Hjellming RM. 1974. *Publ. Astron. Soc. Pac.* 86:616–34

Bally J, O'Dell CR, McCaughrean MJ. 2000. *Astron. J.* 119:2919–59

Bally J, Reipurth B. 2001. *Ap. J.* 546:299–323

Bally J, Sutherland RS, Devine D, Johnstone DD. 1998a. *Astron. J.* 116:293–321

Bally J, Testi L, Sargent A, Carlstrom J. 1998b. *Astron. J.* 116:854–59

Bautista MA, Pradhan AK, Osterbrock DE. 1994. *Ap. J.* 432:L135–38

Bertoldi F, Jenkins EB. 1992. *Ap. J.* 388:495–512

Bertoldi F, Timmermann R, Rosenthal D, Drapatz S, Wright CM. 1999. *Astron. Astrophys.* 346:267–77

Bohlin RC, Hill JK, Stecher TP, Witt AN. 1980. *Ap. J.* 239:137–45

Bonnell I, Kroupa P. 1998. astro-ph/9802306

Brandner W, Grebel EK, Chu Y-H, Dottori H, Brandt B, et al. 2000. *Astron. J.* 119:292–301

Brown AGA, De Geus EJ, De Zeeuw PT. 1994. *Astron. Astrophys.* 289:101–20

Buisson H, Fabry C, Bourget H. 1914. *Ap. J.* 40:241–58

Caillault J-P, Gagnè M, Stauffer JR. 1994. *Ap. J.* 432:386–91

Cardelli JA, Clayton GC. 1988. *Astron. J.* 95:516–25

Castañeda HO. 1988. *Ap. J. Suppl.* 67:93–133
Chen H, Bally J, O'Dell CR, McCaughrean MJ, Thompson RL, et al. 1998. *Ap. J.* 492:L173–76
Churchwell E, Felli M, Wood DOS, Massi M. 1987. *Ap. J.* 321:516–29
Clarke CJ, Bouvier J. 2000. *MNRAS* 319:457–66
Conti PS. 1972. *Ap. J.* 174:L79–86
Costero R, Peimbert M. 1970. *Bol. Obs. Tonant. Tacubaya* 34:229–36
Crutcher RM, Troland TH, Lazareff B, Paubert G, Kazés I. 1999. *Ap. J.* 514:L121–24
Cunha K, Lambert DL. 1994. *Ap. J.* 426:170–91
Cunha K, Lambert DL. 1998. *Ap. J.* 493:195–205
D'Antona F, Mazzitelli I. 1994. *Ap. J. Suppl.* 90:467–500
D'Antona F, Mazzitelli I. 1997. *Mem. Soc. Astron. Ital.* 68:807–30
Duncan DK, Rebull LM. 1996. *Publ. Astron. Soc. Pac.* 108:738–47
Escalante V, Sternberg A, Dalgarno A. 1991. *Ap. J.* 375:630–34
Esteban C, Peimbert M, Torres-Peimbert S, Escalante V. 1998. *MNRAS* 295:401–22
Evans NJ. 1999. *Annu. Rev. Astron. Astrophys.* 37:311–62
Evans NJ, Zuckerman B, Sato T, Morris G. 1975. *Ap. J.* 199:383–97
Feigelson ED, Montmerle T. 1999. *Annu. Rev. Astron. Astrophys.* 37:363–408
Felli M, Churchwell E, Wilson TL, Taylor GB. 1993. *Astron. Astrophys. Suppl. Ser.* 98:137–64
Ferland GJ. 2001. *Publ. Astron. Soc. Pac.* 113:41–48
Ferland GJ, Korista KT, Verner DA, Ferguson JW, Kingdon JB, Verner EM. 1998. *Publ. Astron. Soc. Pac.* 110:761–78
Fischel D, Feibelman WA. 1973. *Ap. J.* 180:801–8
Gagnè M, Caillault J-P, Stauffer JR, Linsky JL. 1997. *Ap. J.* 478:L87–90
Garay G, Moran JM, Reid MJ. 1987. *Ap. J.* 314:535–50
Garmire G, Feigelson ED, Broos P, Hillenbrand LA, Pravdo SH, et al. 2000. *Astron. J.* 120:1426–35
Geier S, Wendker HJ, Wisotzki L. 1995. *Astron. Astrophys.* 299:39–52
Genzel R, Reid MJ, Moran JM, Downes D. 1981. *Ap. J.* 244:884–902
Genzel R, Stutzki J. 1989. *Annu. Rev. Astron. Astrophys.* 27:41–85
Gingerich O. 1982. *Ann. NY Acad. Sci.* 395:308–20
Glassgold AE, Huggins PJ, Shucking EL. 1982. *Ann. NY Acad. Sci.* 395:308–20
Gómez Garrido P, Münch G. 1984. *Astron. Astrophys.* 139:30–36
Goudis C. 1982. *The Orion Complex: A Case Study of Interstellar Matter*. Dordrecht: Reidel. 311 pp.
Goudis C, Hippelein H, Meaburn J, Songsathaporn R. 1984. *Astron. Astrophys.* 137:245–49
Grandi SA. 1975a. *Ap. J.* 196:465–72
Grandi SA. 1975b. *Ap. J.* 199:L43–L46
Greve A, Castles J, McKeith CD. 1994. *Astron. Astrophys.* 284:919–35
Hänel A. 1987. *Astron. Astrophys.* 176:347–57
Hayward TL, Houck JR, Miles JW. 1994. *Ap. J.* 433:L157–63
Hébrard G, Péquignot D, Vidal-Madjar A, Walsh JR, Ferlet R. 2000a. *Astron. Astrophys.* 354L:L79–82
Hébrard G, Péquignot D, Walsh JR, Vidal-Madjar A, Ferlet R. 2000b. *Astron. Astrophys.* 364L:L31–35
Heiles C. 1998. *Ap. J.* 498:689–703
Henney WJ. 1994. *Ap. J.* 427:288–304
Henney WJ. 1998. *Ap. J.* 503:760–79
Henney WJ, Arthur SJ. 1998. *Astron. J.* 116:322–35
Henney WJ, Meaburn J, Raga AC, Massey R. 1997. *Astron. Astrophys.* 324:656–71
Henney WJ, O'Dell CR. 1999. *Astron. J.* 118:2350–68
Herbig GH, Terndrup DM. 1986. *Ap. J.* 307:609–18
Herbst W, Rhode KL, Hellenbrand LA, Curran G. 2000. *Astron. J.* 119:261–80
Hester JJ, Scowen PA, Sankrit R, Lauer TR, Ajhar EA, et al. 1996. *Astron. J.* 111:2349–60
Hillenbrand LA. 1997. *Astron. J.* 113:1733–68

Hillenbrand LA. 1998. *Astron. J.* 116:1816–41
Hillenbrand LA, Carpenter JM. 2000. *Ap. J.* 540:236–54
Hillenbrand LA, Hartmann LW. 1998. *Ap. J.* 492:540–53
Hogerheijde MR, Jansen DJ, van Dishoeck EF. 1995. *Astron. Astrophys.* 294:792–810
Hollenbach DJ, Tielens AGGM. 1997. *Annu. Rev. Astron. Astrophys.* 35:179–215
Howarth ID, Prinja RK. 1989. *Ap. J. Suppl.* 69:527–92
Hu X-H. 1996a. PhD thesis. Rice Univ., Houston, TX
Hu X-H. 1996b. *Astron. J.* 112:2712–17
Hua CT. 1972. *Astron. Astrophys.*, 21:105–9
Isobe S. 1977. *Tokyo Astron. Bull.* 249:2875–83
Jansen DJ, Spaans M, Hogerheijde MR, van Dishoeck EF. 1995. *Astron. Astrophys.* 303:541–53
Jenkins EB, Tripp TM, Todd M, Wozniak PR, Sofia UJ, Sonneborn G. 1999. *Ap. J.* 520:182–95
Johnson HL. 1967. *Ap. J.* 150:L39–43
Johnstone D, Hollenbach D, Bally J. 1998. *Ap. J.* 499:758–76
Jones BF, Walker MG. 1985. *Astron. J.* 90:1320–23
Jones BF, Walker MG. 1988. *Astron. J.* 95:1755–82
Jones MR. 1992. PhD thesis. Rice Univ., Houston, TX
Kaler JB. 1967. *Ap. J.* 148:925–26
Kingdon J, Ferland GJ, Feibelman WA. 1995. *Ap. J.* 439:793–99
Kroupa P. 2000. *New Astron.* 4:615–24
Kroupa P, Petr MG, McCaughrean MJ. 1999. *New Astron.* 4:495–520
Lada CJ, Muench AA, Haisch KE, Lada EA, Alves JF, et al. 2000. *Astron. J.* 120:3162–76
Lada EA, Dutrey A, Guilloteau S, Mundy L. 1996. *Bull. Am. Astron. Soc.* 28:1352
Laques P, Vidal JL. 1979. *Astron. Astrophys.* 73:97–106
Lasker BM. 1966. *Ap. J.* 143:700–21
Laurent C, Vidal-Madjar A, York DG. 1979. *Ap. J.* 229:923–41
Lee J-K, Burton MG. 2000. *MNRAS* 315:11–20
Leibowitz EM. 1973. *Ap. J.* 186:899–907
Leroy JL, Le Borgne JF. 1987. *Astron. Astrophys.* 186:322–32
Lester DF, Dinerstein HL, Rank DM. 1977. *Ap. J.* 232:139–42
Liu X-W, Barlow MJ, Danziger IJ, Storey PJ. 1995. *Ap. J.* 450:L59–62
Lucas PW, Roche PF. 2000. *MNRAS* 314:858–64
Lucas PW, Roche PF, Allard F, Hauschildt PM. 2001. *MNRAS* In press
Luhman KL, Rieke GH, Young ET, Cotera AS, Chen H, et al. 2000. *Ap. J.* 540:1016–40
Massey RM, Meaburn J. 1995. *MNRAS* 273:615–24
Mathews WG. 1965. *Ap. J.* 142:1120–40
Mathews WG, O'Dell CR. 1969. *Annu. Rev. Astron. Astrophys.* 7:67–87
Mathis JS. 1995. *Rev. Mex. Astron. Astrophys.* 3:207–14
Mathis JS, Perinotto M, Patriarch P, Schiffer FH III. 1981. *Ap. J.* 249:99–108
McCaughrean MJ, Mac Low M-M. 1997. *Astron. J.* 113:391–400
McCullough PR, Fugate RQ, Christou JC, Ellerbroek BL, Higgins CH, et al. 1995. *Ap. J.* 438:394–403
Meaburn J. 1988. *MNRAS* 233:791–800
Menton KM, Reid MJ. 1995. *Ap. J.* 445:L157–60
Mezger PG, Wink JE, Zylka R. 1990. *Astron. Astrophys.* 228:95–107
Münch G. 1958. *Rev. Mod. Phys.* 30:1035–41
Münch G. 1985. *Mitt. Astron. Ges.* 63:65–74
Münch G, Persson SE. 1971. *Ap. J.* 165:241–58
Münch G, Taylor K. 1974. *Ap. J.* 192:L93–95
Münch G, Wilson OC. 1962. *Z. Astrophys.* 56:127–37
Mundy LG, Looney LW, Lada EA. 1995. *Ap. J.* 452:L137–40
Myers PC, Goodman AA. 1988. *Ap. J.* 326:L27–30
Ney EP, Allen DA. 1969. *Ap. J.* 155:L193–96
O'Dell CR. 1994. *Astron. Space Sci.* 216:267–80
O'Dell CR. 1998a. *Astron. J.* 115:263–73
O'Dell CR. 1998b. *Astron. J.* 116:1346–56
O'Dell CR. 2000. *Astron. J.* 119:2311–18

O'Dell CR. 2001a. *Publ. Astron. Soc. Pac.* 113:29–40
O'Dell CR. 2001b. *Rev. Mex. Astron. Astrophys.* In press
O'Dell CR, Beckwith SVW. 1997. *Science* 276:1355–59
O'Dell CR, Ferland G, Henney WJ. 2001. *Ap. J.* In press
O'Dell CR, Hartigan P, Bally J, Morse J. 1997. *Astron. J.* 104:2016–28
O'Dell CR, Hubbard WB. 1965. *Ap. J.* 142:591–603
O'Dell CR, Valk JH, Wen Z, Meyer DM. 1993a. *Ap. J.* 405:678–83
O'Dell CR, Walter DK, Dufour RJ. 1992. *Ap. J.* 399:L67–70
O'Dell CR, Wen Z. 1992. *Ap. J.* 387:229–40
O'Dell CR, Wen Z. 1994. *Ap. J.* 436:194–202
O'Dell CR, Wen Z, Hu X. 1993b. *Ap. J.* 410:696–700
O'Dell CR, Wong S-K. 1996. *Astron. J.* 111:846–55
O'Dell CR, Yusef-Zadeh F. 2000. *Astron. J.* 120:382–92
Onaka T, Sawamura M, Tanaka W, Watanabe T, Kodaira K. 1984. *Ap. J.* 287:359–70
Osterbrock DE. 1989. *Astrophysics of Gaseous Nebulae and Active Galactic Nuclei*. Mill Valley, CA. Univ. Sci. Press. 408 pp.
Osterbrock DE, Flather E. 1959. *Ap. J.* 129:26–43
Osterbrock DE, Tran HD, Veilleux S. 1992. *Ap. J.* 389:305–24
Oudmaijer RD, Drew JE, Barlow MJ, Crawford IA, Proga D. 1997. *MNRAS* 291:110–20
Padgett DL, Strom SE, Ghez A. 1997. *Ap. J.* 477:705–10
Pagel BEJ. 1997. *Nucleosynthesis and Chemical Evolution of Galaxies*. Cambridge: Cambrige Univ. Press. 378 pp.
Palla F, Stahler SW. 1999. *Ap. J.* 525:772–83
Palla F, Stahler SW. 2001. *Ap. J.* In press
Pallister WS, Perkins HG, Scarrott SM, Bingham RG, Pilkington JDH. 1977. *MNRAS* 178:P93–95
Pankonin V, Walmsley CM, Harwit M. 1979. *Astron. Astrophys.* 75:34–43
Patriarchi P, Perinotto M. 1985. *Astron. Astrophys.* 143:35–38
Peimbert M. 1967. *Ap. J.* 150:825–34
Peimbert M, Sarmiento A, Fierro J. 1991. *Publ. Astron. Soc. Pac.* 103:815–23
Perinotto M, Patriarchi P. 1980. *Ap. J.* 238:614–19
Petr MG, de Foresto VC, Beckwith SVW, Richichi A, McCaughrean MJ. 1998. *Ap. J.* 500:825–37
Piskunov N, Wood BE, Linsky JL, Depmsey RC, Ayres TR. 1997. *Ap. J.* 474:315–28
Pogge RW, Owen JM, Atwood B. 1992. *Ap. J.* 399:147–58
Prosser CF, Stauffer JR, Hartmann L, Soderblom DR, Jones BF, et al. 1994. *Ap. J.* 421:517–41
Rao R, Crutcher RM, Plambeck RL, Wright MCH. 1998. *Ap. J.* 502:L75–78
Rodríguez-Franco A, Martìn-Pintado J, Wilson TL. 1999. *Astron. Astrophys.* 351:1103–14
Rubin RH, Martin PG, Dufour RJ, Ferland GJ, Baldwin JA, et al. 1998. *Ap. J.* 495:891–904
Rubin RH, Simpson JP, Erickson EF, Haas MR. 1988. *Ap. J.* 327:377–88
Rubin RH, Simpson JP, Haas MRE, Erickson EF. 1991. *Publ. Astron. Soc. Pac.* 103:834–37
Savage BD, Sembach KR. 1996. *Annu. Rev. Astron. Astrophys.* 34:279–330
Schmid-Burgk J, Güsten R, Mauersberger R, Schulz A, Wilson TL. 1990. *Ap. J.* 362:L25–28
Schulz NS, Canizares E, Huenemoerder D, Kastner JH, Taylor SC, Bergstrom EJ. 2001. *Ap. J.* 549:441–51
Seema P. 1996. *Publ. Astron. Soc. Pac.* 108:461–461
Simpson JP, Rubin RH, Erickson EF, Haas MR. 1986. *Ap. J.* 311:895–908
Sorrell WH. 1992. *MNRAS* 255:594–602
Spitzer L. 1978. *Physical Processes in the Interstellar Medium*. New York: Wiley. 318 pp.
Stahl O, Kaufer A, Rivinus T, Szeifert T, Wolf B, et al. 1996. *Astron. Astrophys.* 312:539–48
Stahl O, Mandel H, Wolf B, Gäng T, Kaufer

A, et al. 1993. *Astron. Astrophys.* 274:L29–32
Stassun KG, Mathieu RD, Mazeh T, Vrba FJ. 1999. *Ap. J.* 117:2941–79
Stecklum B, Henning T, Feldt M, Hayward TL, Hoare MG, et al. 1998. *Astron. J.* 115:767–76
Stone JM, Xu J, Mundy LG. 1995. *Nature* 377:315–17
Störzer H, Hollenbach D. 1998. *Ap. J.* 502: L71–74
Störzer H, Hollenbach D. 1999. *Ap. J.* 515:669–84
Strand KA. 1958. *Ap. J.* 128:14–30
Strömgren B. 1939. *Ap. J.* 89:526–47
Swenson FJ, Faulkner J, Rogers FJ, Iglesias CA. 1994. *Ap. J.* 425:286–302
Swings P. 1955. In *Aurorae and the Airglow*, ed. EB Armstrong, A Dalgarno, p. 249. Oxford: Pergamon
Tauber JA, Lis DC, Keene J, Schilke P, Büttgenbach TH. 1995. *Astron. Astrophys.* 297:567–73
Tauber JA, Tielens AGGM, Meixner M, Goldsmith PF. 1994. *Ap. J.* 422:136–52
Tedds JA, Brand PWJL, Burton MG. 1999. *MNRAS* 307:337–56
Tielens AGGM, Hollenbach D. 1985. *Ap. J.* 291:747–54
Tielens AGGM, Meixner MM, van der Werf PP, Bregman J, Tauber JA, et al. 1993. *Science* 262:86–89
Traub WA, Carleton NP, Hegyi DJ. 1974. *Ap. J.* 190:L81–84
Troland TH, Heiles C, Goss WM. 1989. *Ap. J.* 337:342–54
van Altena WF, Lee JT, Lee J-F, Lu PK, Upgren AR. 1988. *Astron. J.* 95:1744–54
van der Werf PP, Goss WM. 1989. *Astron. Astrophys.* 224:209–24
van der Werf PP, Goss WM. 1990. *Ap. J.* 354:157–63
Verner EM, Verner DA, Baldwin JA, Ferland GJ, Martin PG. 2000. *Ap. J.* 543:831–39
von Hörner S. 1951. *Z. Astrophys.* 30:17–64
Walborn NR. 1981. *Ap. J.* 243:L37–39
Walborn NR, Panek RJ. 1984. *Ap. J.* 286:718–24
Walborn NR, Nichols JS. 1994. *Ap. J.* 425:L29–32
Walker MF. 1983. *Ap. J.* 271:642–62
Walmsley CM, Natta A, Oliva E, Testi L. 2000. *Astron. Astrophys.* 364:301–17
Walter DK. 1993. PhD thesis. Rice Univ., Houston, TX
Walter DK, Dufour RJ, Hester JJ. 1992. *Ap. J.* 307:196–213
Warren WH, Hesser JE. 1977. *Ap. J. Suppl.* 34:115–231
Wen Z, O'Dell CR. 1993. *Ap. J.* 409:262–68
Wen Z, O'Dell CR. 1995. *Ap. J.* 438:784–93
White RL, Schiffer FH II, Mathis JS. 1980. *Ap. J.* 241:208–17
Wilson OC, Münch G, Flather EM, Coffeen MF. 1959. *Ap. J. Suppl.* 4:199–256
Wilson TL, Filges L, Codella C, Reich W, Reich P. 1997. *Astron. Astrophys.* 327:1177–84
Wright CM, van Dishoeck EF, Cox P, Sidher SD, Kessler MF. 1999. *Ap. J.* 515:L29–33
Wurm K. 1961. *Z. Astrophys.* 52:149–64
Yorke HW. 1986. *Annu. Rev. Astron. Astrophys.* 24:49–88
Young Owl RC, Meixner MM, Wofire M, Tielens AGGM, Tauber J. 2000. *Ap. J.* 540:886–906
Zapatero Osorio MR, Béjar VJS, Martin EL, Rebolo R, Barrado y Navascués D, et al. 2000. *Science* 290:103–7
Zuckerman B. 1973. *Ap. J.* 183:863–69

Figure 2 This false color image of Orion was compiled from a mosaic of Hubble Space Telescope WFPC2 images (O'Dell & Wong 1996). The color coding, which is true for all other images in this article unless otherwise noted, is blue(F502N-[O III]), green(F656N-Hα), red(F658N-[N II]). The image is 408″ on each side.

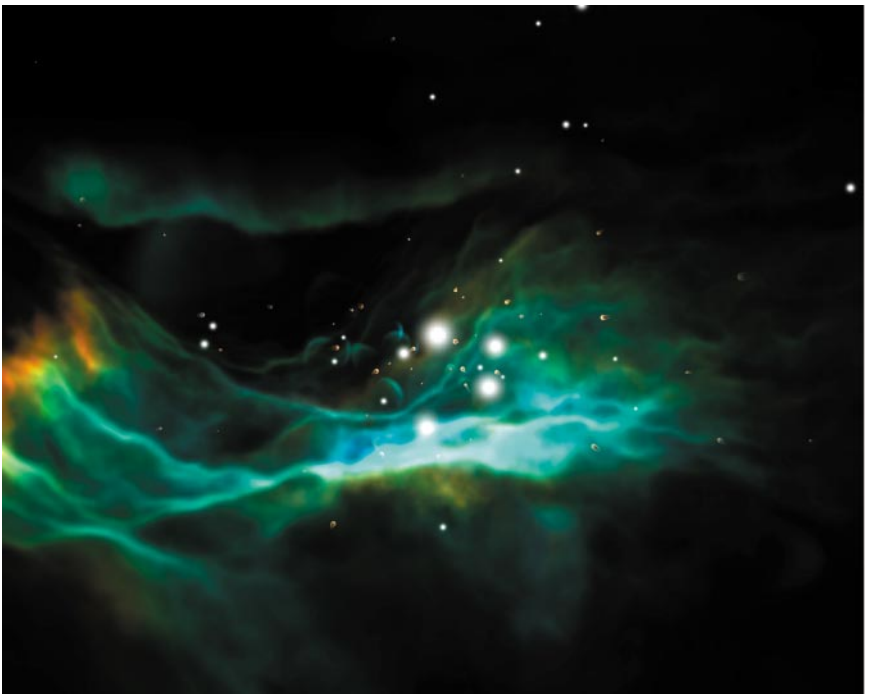

Figure 5 A depiction of the center of the Orion Nebula Cluster and M 42 as viewed from the Southwest. The escarpment which produces the Bright Bar feature is on the far left and the brightest region that lies over the Orion-S molecular outflow source is in the low middle. The relative positions of the stars and proplyds have been determined from the assumption of a symmetric distribution in 3-D as determined by Hillenbrand & Hartmann (1998) except where there is specific evidence for the position. The shocks associated with outflows from low mass stars are shown in positions developed in O'Dell & Bally (2000) and Bally et al. (2000). The distance to the inner side of the foreground Veil (horizontal bright feature above the brightest star, θ^1 Ori C), is probably the most uncertain dimension in this depiction.

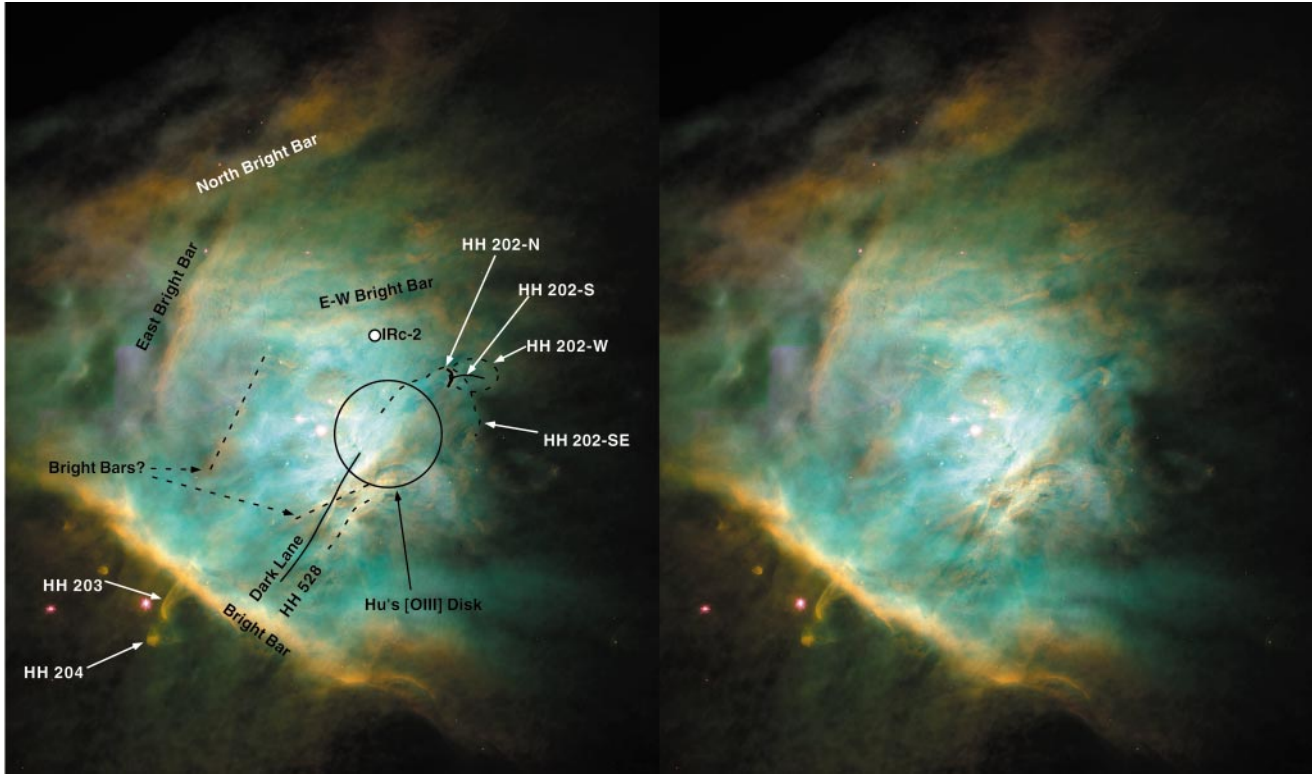

Figure 6 A pair of reduced angular resolution, extinction corrected HST images are shown, the major features discussed in this section are labeled in the left hand panel (O'Dell & Yusef-Zadeh 2000).

Figure 7 This J(blue)H(green),K(red) image (Lada et al. 2000) was made with the 1.2 m Ritchey-Chretien telescope and the STELIRCAM camera at the Fred Lawrence Whipple Observatory on Mt. Hopkins, Arizona and illustrates the tight concentration of the cluster and the greater infrared visibility of the stellar component of the M 42 system.

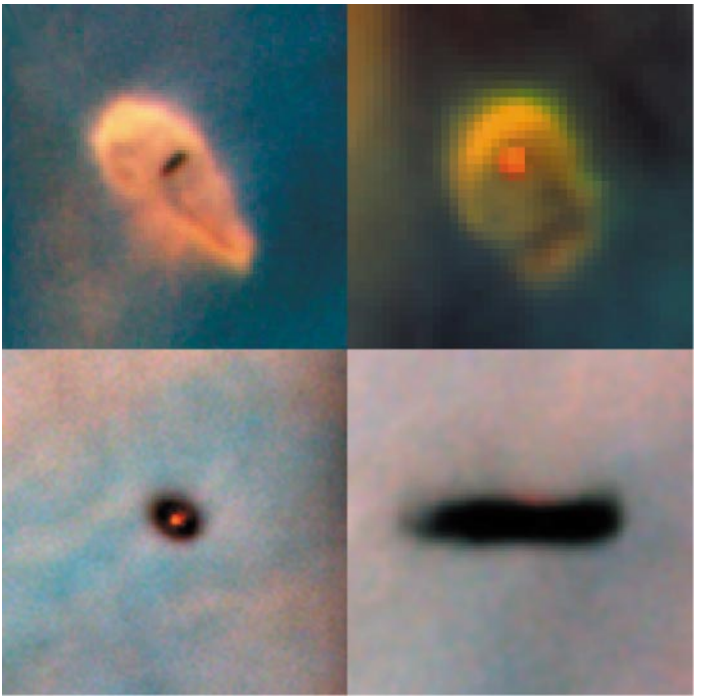

Figure 8 The variety of visibilities of the inner neutral disks are shown in this set of images. Reading clockwise from the upper left, they are 182–413, 206–446, 114–426, and 183–405 (O'Dell & Beckwith 1997). Each figure is 4.1″ square, corresponding to 1800 AU at a distance of 450 pc.

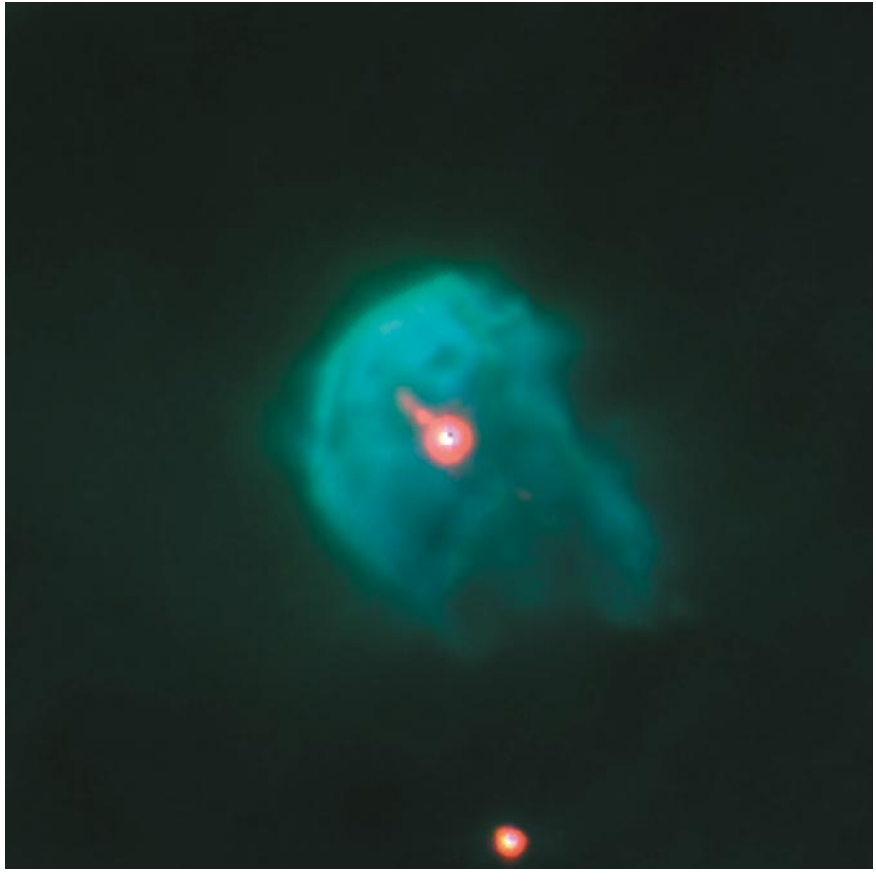

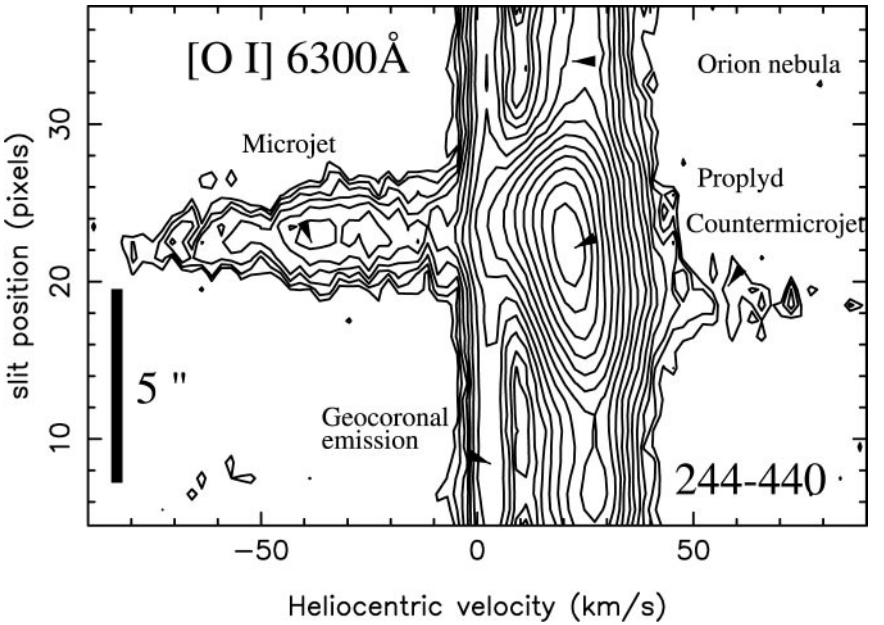

Figure 10 The left hand figure (*opposite page*) shows the largest proplyd 244–440 in Hα (*blue*) and [O I] (*red*), the field size being 11.9″ square. The right hand figure (*above*) shows a Keck slit spectrum across the same object, demonstrating that the brighter jet is blueshifted and the much fainter counterjet is redshifted, these both being seen against the strong night sky and nebular lines. The right hand figure was prepared by Will Henney.

Annual Review of Astronomy and Astrophysics
Volume 39, 2001

CONTENTS